Lithos 148 (2012) 27–44

Contents lists available at SciVerse ScienceDirect

Lithos

journal homepage: www.elsevier.com/locate/lithos

Genesis of the Hengling magmatic belt in the North China Craton: Implications for Paleoproterozoic tectonics

Peng Peng [a,*], Jinghui Guo [a], Mingguo Zhai [a], Brian F. Windley [b], Tiesheng Li [a], Fu Liu [a]

[a] State Key Laboratory of Lithospheric Evolution, Institute of Geology and Geophysics, Chinese Academy of Sciences, Beijing 100029, China
[b] Department of Geology, University of Leicester, Leicester LE1 7RH, UK

ARTICLE INFO

Article history:
Received 3 March 2012
Accepted 22 May 2012
Available online 30 May 2012

Keywords:
North China Craton
Paleoproterozoic
Mafic dyke swarm
Hengling magmatic belt
Intra-continental rift
Tectonics

ABSTRACT

The 2200–1880 Ma igneous rocks in the central and eastern parts of the North China Craton (NCC) constitute a new Hengling magmatic belt (HMB), which includes the ~2147 Ma Hengling mafic sill/dyke swarm, the ~2060 Ma Yixingzhai mafic dyke swarm, and the ~1973 Ma Xiwangshan mafic dyke swarm. The three swarms are contiguous and have experienced variable degrees of metamorphism from greenschist to low amphibolite facies (Hengling), medium granulite facies (Yixingzhai), and medium/high-pressure granulite facies (Xiwangshan). They are all tholeiitic in composition typically with 47–52 wt.% SiO_2 and 4–10 wt.% MgO, and all show light rare earth element enrichments and Nb- and Ta-depletion. Their Nd T_{DM} ages are in the range of 2.5–3.0 Ga. Specifically, the Hengling and Yixingzhai dykes/sills are depleted in Th, U, Zr, Hf and Ti, whereas the Xiwangshan dykes are enriched in U and weakly depleted in other elements. Variable Sr-anomalies indicate significant feldspar accumulation (positive anomalies) or fractionation. The $\varepsilon Nd_{(t)}$ values of the three swarms are: −3.2–+3.0 (Hengling), −1.7–+1.8 (Yixingzhai) and −1.4–+1.0 (Xiwangshan).

These mafic representatives of the HMB originated from the >2.5 Ga sub-continental lithospheric mantle of the NCC, and with A-type granites and other igneous associations in this belt they likely evolved in an intra-continental rift. The progressive changing compositions of the three swarms are interpreted in terms of their source regions at different depths, i.e., shallower and shallower through time. And the decrease in scale and size of the intrusions and their magma volumes indicate the progressive weakening of magmatism in this rift. The rocks in this belt are different chronologically, petrologically and chemically from those in the Xuwujia magmatic belt (XMB). We propose that the two magmatic belts represent two different magmatic systems in different blocks of the NCC, i.e., an eastern block (with the HMB) and a western block (with the XMB). Terminal collision was possibly a result of ridge subduction between the two blocks, which led to exhumation of the igneous rocks in the two belts from different crustal levels, distinguishable by their different grades of metamorphism.

1. Introduction

The North China Craton (NCC) in eastern Asia covers most of northern China and part of the Korean Peninsula with a total area of ~1 500 000 km^2 (Fig. 1). It has a crustal record back to 3.8 Ga (Liu et al., 2008; Wu et al., 2008), and experienced major orogenic events at ca. 2.5 Ga represented by widespread gneisses of tonalite–trondhjemite–granodiorite (TTG) composition and metamorphism up to medium-pressure granulite facies, and at 1.93–1.80 Ga manifested by high-grade metamorphism up to high-pressure granulite facies and ultrahigh-temperature granulite facies (Guo et al., in press; Kusky and Li, 2003; Santosh et al., 2007a,b; Wan et al., 2010; Zhai and Liu, 2003; Zhai et al., 1993; Zhao et al., 2001, 2005). At ca. 1.78 Ga there was intrusion of a craton-scale mafic dyke swarm, after which there was little deformation and metamorphism (Peng et al., 2008 and references therein). Controversial issues revolve around the tectonic interpretation of the 2.5 Ga and 1.9–1.8 Ga events and the processes that give rise to the Craton, especially in the Late Paleoproterozoic, although it is widely proposed that the NCC formed as a result of the amalgamation of Neoarchean blocks (see Fig. 1).

Four main models have been proposed: 1. The final amalgamation took place at ca. 1.85 Ga along a high-pressure metamorphic belt between a western block (previously amalgamated from two smaller sub-blocks at 2.0–1.9 Ga), and an eastern block within which a rift in the east had opened and closed between 2.2 Ga and 1.9 Ga (Guo et al., 2005; Kröner et al., 2005, 2006; Liu et al., 2005; Santosh et al., 2007a,b, 2012a,b; Wilde et al., 2002; Zhang et al., 2007, 2012; Zhao et al., 2001, 2002a, 2005, 2008a). 2. There are two Late Paleoproterozoic suture zones in the center of the NCC, i.e., the

* Corresponding author. Tel.: +86 10 82998530.
E-mail addresses: pengpengwj@mail.iggcas.ac.cn, pengpengwj@hotmail.com (P. Peng).

0024-4937/$ – see front matter © 2012 Elsevier B.V. All rights reserved.
doi:10.1016/j.lithos.2012.05.021

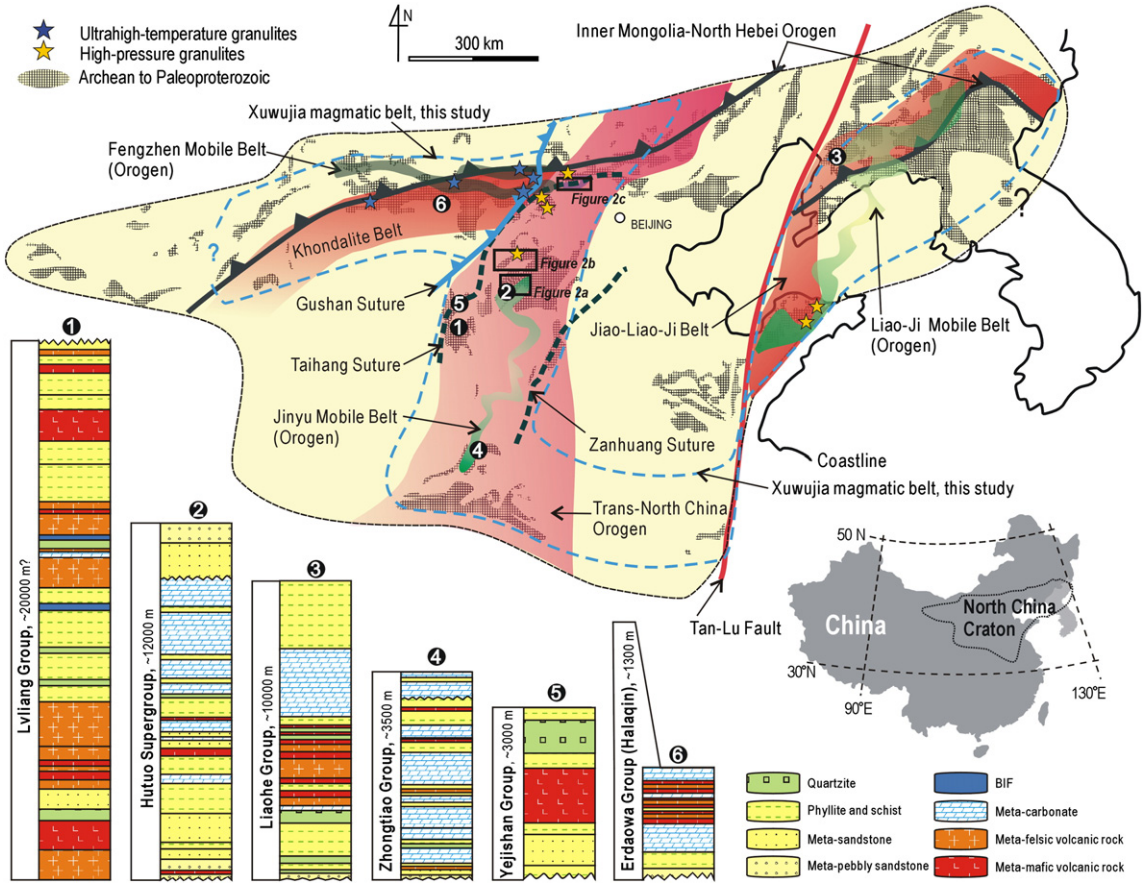

Fig. 1. A simplified Precambrian geological map of the North China Craton, with its different Paleoproterozoic tectonic subdivisions: Trans-North China Orogen, Khondalite and Jiao–Liao-Ji Belts by Zhao et al. (2005, 2011); the Fengzhen, Jinyu, and Liao-Ji mobile belts by Zhai and Liu (2003); Inner-Mongolia-North Hebei Orogen by Kusky and Li (2003) and Kusky et al. (2007); Taihang and Zanhuang Sutures by Trap et al. (2012); and Gushan Suture of Peng et al. (2012a). Also shown are strata of typical Paleoproterozoic volcano-sedimentary sequences in the North China Craton, e.g., the Hutuo, Lvliang, Yejishan, Zhongtiao, Liaohe and Erdaowa (Halaqin) Groups . The numbers (1 to 6) in the NCC indicate the localities of the individual stratigraphic columns.
The strata of the typical Paleoproterozoic volcano-sedimentary sequences in the North China Craton are revised after Du et al. (2010, 2011), Geng et al. (2000), GSBS (2002), Jiang (1987), Liu et al. (2012), Peng et al. (2011), Sun and Hu (1993), Yu et al. (1997), Zhang et al. (2010) and Zhao et al. (2008b).

Taihang and Zanhuang sutures, which closed sequentially between 2.1 Ga and 1.8 Ga (Trap et al., 2007, 2011, 2012). 3. Amalgamation in the end-Archean (ca. 2.5 Ga) was followed by subduction and collision along the northern margin of the NCC in the Late Paleoproterozoic (ca. 1.85 Ga) (Kusky and Li, 2003; Kusky et al., 2007; Li et al., 2000). 4. Cratonization of the NCC at 2.7–2.5 Ga, which gave rise to several greenstone belts that separate Archean nuclei, was followed by reworking of different rifts and mobile belts in the period 2.2–1.9 Ga (Zhai and Liu, 2003; Zhai and Santosh, 2011; Zhai et al., 1993). All data, and these models on which they are based, indicate that the NCC experienced complicated tectonic processes in the Late Paleoproterozoic, which according to some authors resulted from the assembly of a Paleoproterozoic (2.0–1.9 Ga) supercontinent (Santosh, 2010; Wilde et al., 2002; Zhao et al., 2002b).

Although metamorphic, geochemical, isotopic and structural work has improved our understanding of the Late Paleoproterozoic evolution of the NCC, systematic studies of the igneous rocks and their tectonic environments are still insufficient, in particular, the geometry and petrogenesis of mafic dykes, which are useful to constrain the tectonic environment (e.g., Hanski et al., 2006), because they typically have a short lifespan and undergo little crustal assimilation, and therefore tend to preserve well their original chemical characteristics, in spite of later metamorphism. Relevant in this regard are 1.95–1.88 Ga contemporaneous magmatic rocks in the western block of the NCC, which have a close genetic relationship with in-situ ultrahigh-temperature metamorphism; they include gabbronorites, charnockites, S-type granites, and volcano-sedimentary rocks; the mineralogy, petrology and *PT* data of which were best explained by a model of ridge subduction (Guo et al., in press; Peng et al., 2010, 2011, 2012a) (Fig. 1).

The NCC contains minor igneous rocks with ages between 2400 and 2200 Ma, but abundant 2200–1600 Ma igneous rocks (Supplement data Table 1 and references listed). Specifically at 1880–1790 Ma, the NCC underwent a regional high-pressure granulite facies metamorphism, which was followed by a widespread amphibolite facies retrogression (Dong et al., 2010; Guo et al., 2005; Liu et al., 1998; Tam et al., 2010; Xie et al., 2011; Zhai et al., 1993; Zhao et al., 2001; Zhou et al., 2008) that was accompanied by 1880–1790 Ma granitic rocks (Geng et al., 2004; Lu et al., 2006; Wilde et al., 2002; Zhao et al., 2006, 2008a). Subsequently, a swarm of giant craton-scale mafic dyke swarm was intruded at ~1780–1770 Ma, and followed by the emplacement of several generations of smaller mafic dykes and volcanic rocks with ages as young as ~1600 Ma (Peng et al., 2008 and references therein).

Except for the relatively well-documented 1880–1600 Ma mostly granitic rocks and mafic dyke swarms, the 2200–1880 Ma magmatism is of special importance in the Paleoproterozoic evolution of the Craton, and yet relatively little is known about it. In this paper we present new geochemical and isotopic age data on several generations of 2200–1880 Ma dykes/sills, and propose that they occur in a Paleoproterozoic intracontinental rift within a newly-defined coeval magmatic belt. This new information should help in understanding and unraveling the complex framework and evolution of this classic craton.

2. 2200–1880 Ma igneous rocks in the North China Craton

The 2200–1880 Ma igneous rocks in the NCC include volcanic lavas and tuffs, granitic plutons, and mafic dykes, sills and plutons (Supplement data Table 1). Representative volcanic rocks occur in the center of the NCC in the Hutuo, Lvliang (also spelled as Lüliang or Luliang), Yejishan and Zhongtiao (Super-) Groups/Complexes, in the Liaohe Group, Guanghua, Laoling and Ji'an Groups in the east, and in the Erdaowa Group (Halaqin volcanics) in the west (Fig. 1). These volcanic rocks are of variable thickness and are intercalated with clastic- and carbonate-dominated sediments, they vary in composition from basalts and andesites, to rhyolites and dacites, with common pillow lavas and lithic tuffs, and their metamorphic grade ranges from low greenschist to high amphibolite facies (Du et al., 2010, 2011; Geng et al., 2000; Jiang, 1987; Li et al., 2012; Liu et al., 2011, 2012; Lu et al., 2006; Peng et al., 2011; Sun and Hu, 1993; Wilde et al., 2003; Yu et al., 1997; Zhang et al., 2010; Zhao et al., 2008b). In addition, the Liaohe Group contains the most important Mg and Mg–Fe borate deposits in China (Peng and Palmer, 2002).

The 2200–1880 Ma granitic rocks include a variety of granodiorites, charnockites, tonalites, monzogranites, biotite granites and garnet/sillimanite-bearing granites (Geng et al., 2000; Guo and Li, 2009; Kröner et al., 2005; Li and Zhao, 2007; Li et al., 2012; Liu et al., 2009b; Lu et al., 2004a,b; Peng et al., 2012a; Wan et al., 2006; Wang and Wilde, 2002; Wang et al., 2010c; Wilde, 1998; Wu et al., 2007; Yang et al., 2009, 2011; Zhao et al., 2002a, 2006, 2008a,b, 2011). Some of these granitic rocks are deformed with gneissic schistosity conformable with that of their host rocks (e.g., Mafeng monzogranites, Li and Zhao, 2007; tonalites in the Jiehekou Group/Complex, Zhao et al., 2008b); whereas others are largely undeformed (e.g., Tonghua A-type granites, Lu et al., 2004b; and Lingyunkou A-type granites, Zhao et al., 2011). Granodiorites and tonalites are mostly in the center of the NCC (Geng et al., 2000; Kröner et al., 2005; Liu et al., 2009b; Wang et al., 2010c; Wilde, 1998; Wilde et al., 2005; Zhao et al., 2008a,b, 2011), charnockites are in the west (Peng et al., 2012a), monzogranites and biotite granites are mostly in the east (Guo and Li, 2009; Lu et al., 2004a,b; Wu et al., 2007; Zhao et al., 2006), with some in the center (Geng et al., 2000; Zhao et al., 2002a), and S-type granites are mainly in the west (Peng et al., 2012a). Some 1930–1880 Ma aluminum-rich (S-type?) granitic gneisses (e.g., sillimanite-garnet granite, garnet monzogranite, biotite granite, etc.) in North Korea are along the eastern boundary of the NCC (Wu et al., 2007; Zhao et al., 2006).

The mafic intrusive rocks in the NCC are mostly dykes, with a few sills and small plutons (e.g., Guo et al., 2005; Peng et al., 2005, 2010; Wang et al., 2010c). There are also ~1.95 Ga carbonatite dykes in the west (Wan et al., 2008). These sills/dykes have mostly undergone greenschist to amphibolite to granulite facies metamorphism, e.g., amphibolite facies in the Hengling area (Peng et al., 2005), medium-pressure granulite facies in the Yixingzhai area (O'Brien et al., 2005), high-pressure granulite facies in the Xiwangshan area (e.g., Guo et al., 2005; Peng et al., 2005); and high-temperature granulite facies metamorphism in the Xuwujia area (e.g., Peng et al., 2010). In this study, we have investigated three generations of dykes/sills, namely the Hengling, Yixingzhai and Xiwangshan, with different metamorphic grades. Although they are deformed and metamorphosed, their igneous textures are well preserved (O'Brien et al., 2005; Peng et al., 2005). Of the three swarms, the Hengling and Xiwangshan have ages of 2147 ± 5 Ma and 1973 ± 4 Ma (Peng et al., 2005); but the Yixingzhai swarm has not been dated.

3. Occurrence and petrography

3.1. The Hengling sills and dykes

The Hengling sills/dykes intruded the ~2.5 Ga Wutai greenstone belt (or supracrustal rocks) and the Paleoproterozoic Hutuo Supergroup (a volcano-sedimentary sequence, see the stratigraphic column in Fig. 1) (Fig. 2a). They occur mostly as sills (Fig. 3a) with minor dykes and small stocks; the longest Liudingsi sill is ~30 km long and up to 400 m thick (Fig. 2a). They have chilled margins, and relic igneous textures are preserved both in the margins and centers (Fig. 3g–j). They have undergone greenschist to low amphibolite facies metamorphism, with a typical mineral assemblage of plagioclase, hornblende (with relic clinopyroxene) and chlorite (Peng et al., 2005; Fig. 3g–j). They are deformed and have a dominant NW–SW to E–W-trending foliation. One mafic dyke from Hengling village has a zircon SHRIMP U–Pb age of 2147 ± 5 Ma (average $^{207}Pb/^{206}Pb$ age) (Peng et al., 2005), which is close to the age of 2140 ± 14 Ma (zircon SHRIMP $^{207}Pb/^{206}Pb$ age (Du et al., 2010)) of a basaltic andesite in the Hutuo Supergroup; dykes of similar age occur in the northeast of the NCC in Jilin province (the Chibaisong dykes, GSBJ, 2004).

3.2. The Yixingzhai dykes

The Yixingzhai dykes occur in the Hengshan Mts. and intruded both the ~2.5 Ga Wutai greenstone belt (locally called the Yixingzhai supracrustal rocks) and the Hengshan gray gneisses (GSBS, 2002; Fig. 2b). They have chilled margins and apophyses (Fig. 3b–d). Although the dykes have undergone medium-pressure granulite facies metamorphism (O'Brien et al., 2005), relict ophitic textures composed of plagioclase laths (Fig. 3k–l) are well preserved. They mainly consist of plagioclase, hornblende and clinopyroxene, with or without metamorphic orthopyroxene and garnet between the matrix plagioclase and clinopyroxene. The Yixingzhai dykes vary from meters to tens of meters in width, and they are mostly deformed as elongate lenses that are hundreds of meters long in wall-rock gneisses, which also have an E–W trending foliation.

3.3. The Xiwangshan dykes

The Xiwangshan dykes are in the ~2.5 Ga Chongli Complex and Huai'an gneisses in the Huai'an–Xuanhua area (Fig. 2c). They are deformed and have no chilled margins; however, their tabular shape and preserved bayonet-like apophyses indicate that they were dykes (Fig. 3e, f). They have undergone medium- to high-pressure granulite facies metamorphism (Guo et al., 2005; Zhai et al., 1993), and their typical mineral assemblage is: clinopyroxene, orthopyroxene, garnet, plagioclase, and variable amounts of amphibole (Peng et al., 2005; Fig. 3m, n). Coarser-grained dykes generally contain more amphiboles than finer-grained dykes (e.g., Fig. 3n, compared with Fig. 3m). The dykes are about 1 to 2 m in width, irrespective of their deformation, and they are up to 2 km long. Their main trend is E–W but a few dykes strike NE–SW and NW–SE. A dyke from the Xiwangshan village contains zircons, the cores of which have a U–Pb zircon SHRIMP age of 1973 ± 4 Ma (Fig. 2e, sample 03XWS01), interpreted as the time of crystallization (Peng et al., 2005). Another dyke from Manjinggou has a similar LA-ICP-MS age of 1964 ± 38 Ma (Wang et al., 2010a). In the Hengshan Mts., Kröner et al. (2006) reported SHRIMP zircon U–Pb ages of 1914 ± 2 Ma and 1915 ± 4 Ma for two of these high-pressure granulite-facies mafic dykes; however, the interpretation of these ages is doubtful according to the morphology of their zircons.

4. Analytical methods

Zircons were separated using standard heavy liquid techniques, and were selected and mounted in an epoxy resin together with standard Temora 1 zircons (conventional ID-TIMS $^{206}Pb/^{238}U$ age = 417 Ma, Black et al., 2003). The mount was polished to expose the centers of the grains, and then gold-coated. Cathodoluminescence electron images were acquired, using a scanning electron microscope at the Beijing SHRIMP Center, in order to examine their internal structures. Zircon

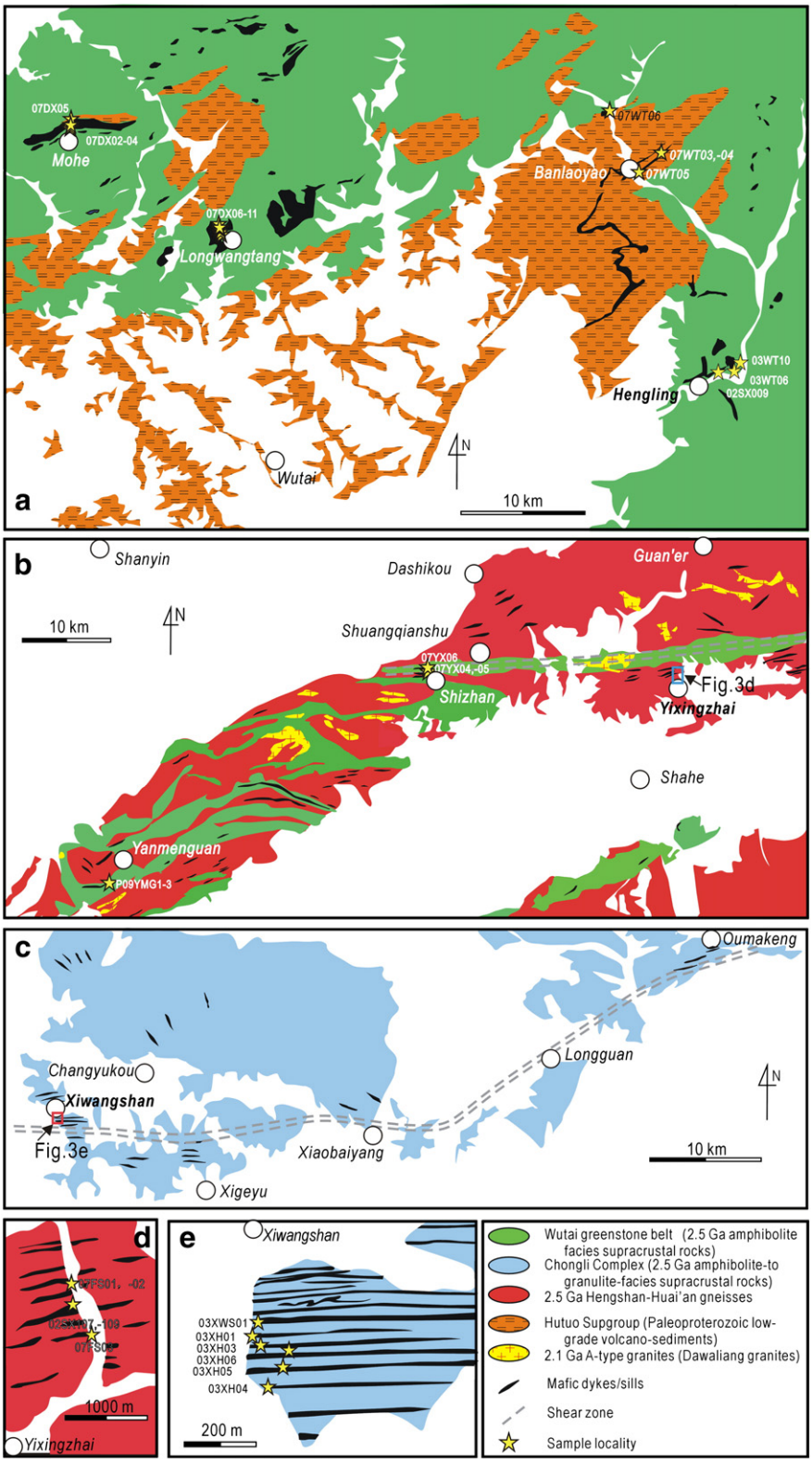

Fig. 2. Simplified geological maps showing (a) the Hengling sills/dykes, (b, d) Yixingzhai dykes, and (c, e) Xiwangshan dykes in the central part of the North China Craton. See Fig. 1 for the locations of these maps.

U–Pb isotope analyses (Supplement data Table 2) were carried out with a SHRIMP-II instrument. Procedures were similar to those in Williams (1998). The diameter of the analytical ion beam at the sample surface was approximately 30–40 μm. Common Pb was corrected using the measured ^{204}Pb. The data in Supplement data Table 2 were processed using the Squid 1.02 and Isoplot 3.0 programs and given 1σ errors.

In situ Hf isotope analyses of zircons (Supplement data Table 3) were determined using a Neptune MC-ICP MS in the State Key Laboratory of Lithospheric Evolution (SKLLE), Beijing. An ~30 μm spot size was applied during ablation with a 193 nm laser. During analysis, isobaric interference corrections of ^{176}Lu on ^{176}Hf were not processed due to the extremely low ^{176}Lu/^{177}Hf ratios in the zircons

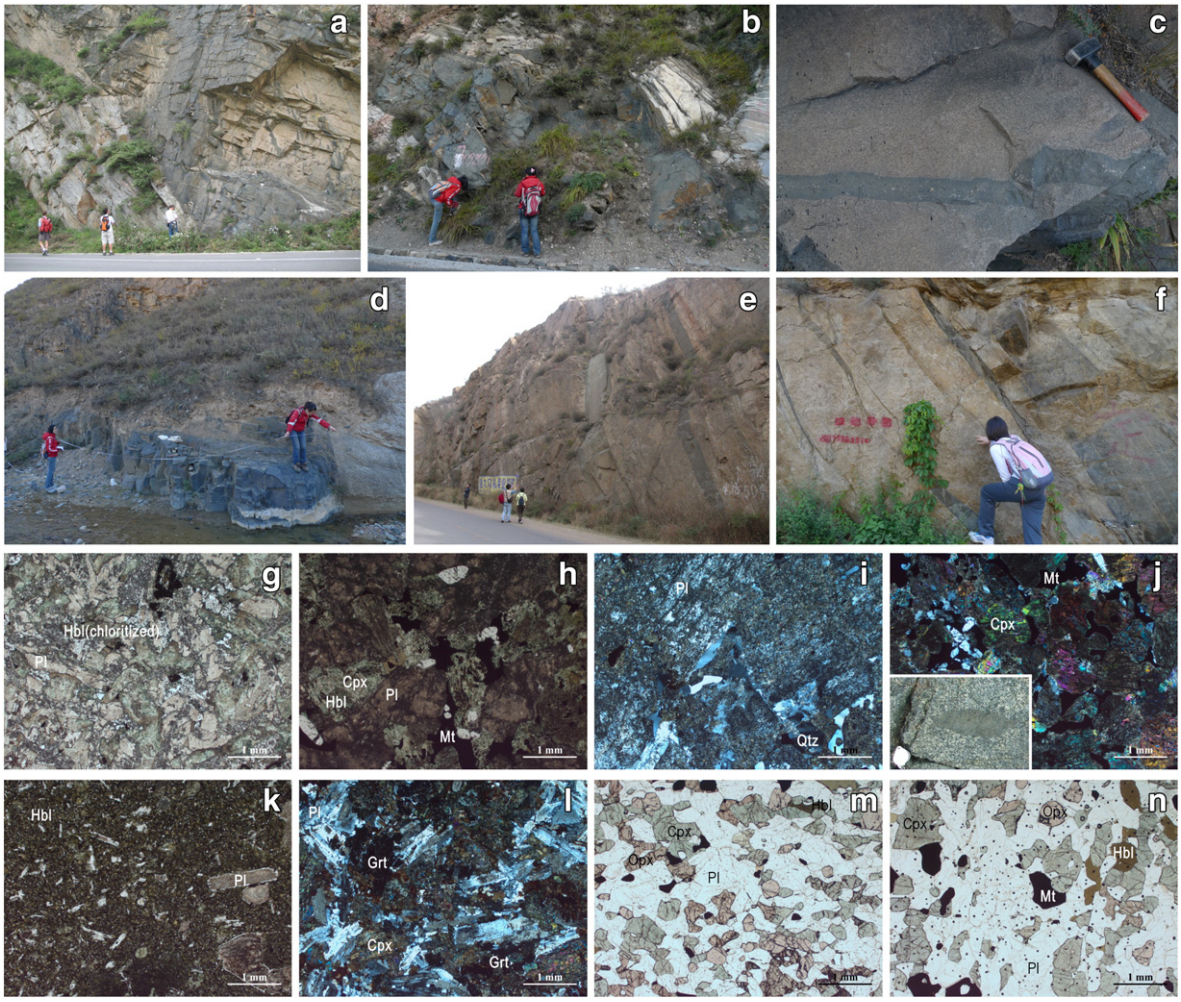

Fig. 3. Selected photos showing outcrops and typical micro-textures of the Hengling sills/dykes in the Wutai Mts. (the Huangtuzhui sill (a); samples 07DX08 (g), 07DX07 (h), 07DX11 (i) and 07DX10 (j; inset: outcrop showing an enclave) are representatives of the chilled margin, center, leucogabbro vein, and pyroxenite enclave of the Longwangtang sill), the Yixingzhai dykes in the Hengshan Mts. (Yanmenguan dyke (b–c), c shows a dykelet inside the main body of the dyke; Yixingzhai dyke (d); samples P09YMG3 (k) and P09YMG1 (l) are from the chilled margin and center of the Yanmenguan dyke, respectively), and the Xiwangshan dykes in the Yinshan Mts. (Xiwangshan (e–f); samples 03XH01 (m) and 03XWS01 (n) are from fine-grained and coarse-grained dykes, respectively). Scale in c is a hammer about 30 cm long, in j inset is a lens about 2.5 cm in diameter, and scales in a, b, d, e and f are persons about 160–190 cm tall. Hbl: hornblende; Cpx: clinopyroxene; Pl: plagioclase; Mt: magnetite; Qtz: quartz; Opx: orthopyroxene; Grt: garnet.

(<0.002), although $^{175}Lu/^{176}Lu = 0.02655$ was used for elemental fractionation correction. The isobaric interference of ^{176}Yb on ^{176}Hf was corrected using the mean fractionation index proposed by Iizuka and Hirata (2005). A value of 0.5886 was used for the $^{176}Yb/^{172}Yb$ ratio (Chu et al., 2002). The data reported here were corrected assuming a $^{176}Hf/^{177}Hf$ ratio of 0.282305 for zircon 91500 (after Wu et al., 2006).

Samples were selected for analyses of their bulk whole-rock compositions and Sr–Nd isotopes in the SKLLE (Beijing). Major elements were determined by X-ray fluorescence (Shimadzu XRF-1700/1500) after fusion with lithium tetraborate using the Chinese national standard samples GBW07101–07114. The precision was better than 0.2 wt.% in the analysis range. Loss on ignition was measured as the weight loss of the samples after 1 hour baking at a constant temperature of 1000 °C. Trace element analyses were determined with an ELEMENT ICP-MS after $HNO_3 + HF$ digestion of about 40 mg of sample powder in a Teflon vessel, with accuracy and reproducibility monitored using the Chinese national standard sample GSR3 (basalt). The relative standard deviation was better than 5% above the detection limits. Data are shown in Table 1.

Sr–Nd isotope determinations (Table 2) were made on a Finnigan MAT 262 spectrometer. NBS987 (Sr standard) and Ames (Nd standard) reference materials were used to constrain analytical bias; however, no adjustment was applied to the unknowns as the measurements of the standards agreed with the standard values within error during the analyses. Procedure backgrounds for Rb–Sr and Sm–Nd isotope analyses were better than 100 and 50 pg, respectively. The external precisions (2σ) of $^{87}Rb/^{86}Sr$ and $^{147}Sm/^{144}Nd$ ratios were both better than 0.5%.

5. Zircon U–Pb and Lu–Hf results

Less than 20 zircon grains were separated from a ~10 kg sample (number 02SX109) from one Yixingzhai dyke in the Yixingzhai village, Hengshan Mts. (Figs. 2b–d and 3d). These grains have lengths of about 100 μm or smaller. Two types of grains, either idiomorphic with clear zones, or irregular with misty internal textures (Fig. 4 inset), were analyzed. The two idiomorphic grains have distinctly high U and Th contents (U at 3392 ppm and 2663 ppm, and Th at 11 446 ppm and 7696 ppm respectively), and high Th/U ratios (3.49 and 2.99); whereas irregular grains have distinctively lower U and Th contents (U at 92–1644 ppm, Th at 4 to 5430 ppm) and variable Th/U ratios (0.04 to 3.41) (Supplement data Table 2).

U–Th–Pb analyses were acquired using the SHRIMP ion probe. The two idiomorphic grains gave $^{207}Pb/^{206}Pb$ ages of 2035.0 ± 6.0 Ma and

Table 1
Major (wt.%) and trace (ppm) element data of the Hengling, Yixingzhai and Xiwangshan dykes/sills in the North China Craton.
Major element data of samples 02SX009 (SX009) and 03XWS01 (XWS01) are cited from Peng et al. (2005).

Number	02SX009	03WT06	03WT10	07DX02	07DX03	07DX04	07DX05	07DX06*	07DX07*	07DX08	07DX09	07DX10**	07DX11***	07WT06	07WTP3	07WTP4	07WTP5
Name	Hengling dyke	Hengling sill	Menxianshi sill	Mohegou sill				Longwangtang sill (stock)						Huangtuzhui sill	Banlaoyao sill		
SiO_2	48.75	49.58	48.01	48.78	48.98	48.38	48.82	47.38	47.31	50.06	49.97	45.27	56.59	49.76	49.38	48.37	50.72
TiO_2	0.55	0.77	0.47	0.98	0.99	0.99	0.94	1.72	1.71	0.92	0.91	1.85	1.09	0.87	0.89	0.68	0.77
Al_2O_3	15.83	15.37	16.88	15.55	15.53	15.14	15.41	16.42	15.52	13.16	13.08	2.05	16.29	13.23	15.67	16.30	14.54
FeO_t	13.1	13.8	11.0	11.4	11.4	12.0	11.5	12.8	13.4	13.8	13.8	19.6	7.9	13.6	12.6	11.1	11.2
MnO	0.17	0.18	0.14	0.17	0.17	0.18	0.17	0.15	0.18	0.19	0.18	0.24	0.09	0.18	0.18	0.13	0.17
MgO	7.98	6.61	9.88	7.55	7.80	8.22	7.89	5.45	5.88	6.77	6.64	13.26	3.27	7.41	6.80	7.99	8.00
CaO	7.58	7.95	8.05	10.89	10.32	10.38	10.95	9.09	8.55	9.55	10.18	15.32	5.74	9.33	8.16	8.65	7.64
Na_2O	2.89	2.21	2.66	2.46	2.62	2.16	2.16	2.90	3.08	2.28	2.58	0.14	3.43	1.76	2.61	2.39	2.73
K_2O	0.40	1.54	0.64	0.39	0.49	0.34	0.24	0.31	1.09	0.47	0.56	0.04	1.79	0.43	1.36	1.35	1.33
P_2O_5	0.14	0.19	0.11	0.10	0.10	0.09	0.09	0.65	0.65	0.10	0.12	1.30	0.41	0.09	0.19	0.15	0.14
LOI	2.52	1.33	2.27	1.22	0.98	1.58	1.30	2.64	2.26	2.48	1.94	0.88	2.82	3.08	1.82	2.32	2.54
Total	99.86	99.54	100.12	99.44	99.40	99.47	99.41	99.55	99.59	99.80	99.91	99.91	99.45	99.71	99.68	99.42	99.78
Rb	11.4	32.0	23.9	7.43		5.39		5.25	29.5	12.0	15.3	0.06		8.53	33.5	25.1	
Sr	446	342	374	384		216		756	678	235	302	78.9		150	253	264	
Ba	76.7	339	281	191		135		222	275	123	146	36.6		59.3	349	216	
Th	0.54	0.95	1.14	0.83		0.83		0.27	0.65	0.55	0.57	0.94		0.72	0.72	0.65	
U	0.14	0.22	0.36	0.24		0.22		0.08	0.16	0.13	0.15	0.23		0.16	0.18	0.19	
Pb	3.91	3.48	3.20	7.34		4.98		6.61	4.74	2.53	2.39	3.99		2.93	2.74	3.96	
Zr	49.8	66.3	42.0	75.0		74.3		30.1	45.0	67.8	69.8	64.0		60.3	93.6	70.5	
Hf	1.51	1.91	1.24	2.17		2.13		0.96	1.38	1.98	2.06	2.59		1.76	2.50	1.97	
Nb	2.13	3.84	4.06	3.21		3.18		7.28	8.28	3.15	3.23	3.00		2.95	4.56	3.41	
Ta	0.35	0.8	0.81	0.20		0.19		0.44	0.53	0.19	0.19	0.17		0.17	0.24	0.18	
Sc	21.2	–	–	32.2		33.0		20.7	22.2	48.1	47.6	59.1		45.7	29.4	25.2	
V	127	–	–	245		244		250	271	306	300	429		260	189	153	
Cr	35.2	74.8	39.8	150		154		93.5	114	115	98.3	316		151	171	267	
Co	79.8	46	49.7	53.0		54.1		40.3	39.1	53.9	52.7	67.4		50.4	51.0	49.8	
Ni	237	83.3	200	179		142		100	121	60.0	56.2	272		63.6	142	156	
Cu	101	98.9	38.3	114		88.8		110	19.9	82.9	75.7	33.6		97.3	83.5	73.5	
Be	0.32	—	—	0.53		0.53		0.74	0.82	0.52	0.53	0.54		0.48	0.64	0.49	
Ga	15.3	16.5	13.7	19.6		18.0		22.6	21.7	16.2	16.4	12.6		15.1	18.5	15.8	
Cs	0.23	1.17	1.02	0.28		0.32		0.38	0.75	0.34	1.05	0.25		0.67	2.93	1.92	
Li	18	—	—	10.2		11.0		14.5	12.7	15.3	12.8	3.06		12.7	30.1	25.5	
La	10.1	14.1	10.5	6.76		5.42		27.2	34.7	7.34	7.96	43.2		6.30	12.9	9.60	
Ce	20.8	31.7	22.5	16.0		12.5		67.6	86.4	16.4	17.9	124		14.6	29.7	21.9	
Pr	2.83	4.04	2.87	2.25		1.89		10.0	12.9	2.32	2.45	21.9		2.05	3.97	2.94	
Nd	11.7	17.6	12.0	10.3		8.60		41.2	51.5	10.4	10.9	97.1		8.99	16.8	12.1	
Sm	2.50	3.52	2.24	2.98		2.46		8.61	10.6	2.85	2.90	22.0		2.47	4.00	2.87	
Eu	0.83	1.05	0.71	1.07		0.80		2.56	2.83	0.98	1.03	2.99		0.85	1.32	0.86	
Gd	2.20	3.41	2.05	3.16		2.93		6.41	7.79	3.49	3.47	16.9		3.08	3.70	2.76	
Tb	0.37	0.56	0.35	0.55		0.52		0.85	0.97	0.64	0.64	2.27		0.55	0.60	0.44	
Dy	2.23	3.29	2.05	3.47		3.33		3.94	5.01	4.18	4.23	12.0		3.82	3.90	2.72	
Ho	0.46	0.74	0.44	0.71		0.66		0.68	0.88	0.89	0.89	2.16		0.82	0.84	0.57	
Er	1.35	2.14	1.25	1.87		1.82		1.65	2.15	2.58	2.51	4.96		2.32	2.32	1.49	
Tm	0.22	0.32	0.20	0.27		0.27		0.22	0.29	0.38	0.38	0.64		0.35	0.34	0.23	
Yb	1.44	2.17	1.27	1.75		1.66		1.40	1.84	2.53	2.51	3.94		2.22	2.16	1.47	
Lu	0.22	0.34	0.21	0.27		0.25		0.20	0.27	0.39	0.39	0.56		0.34	0.33	0.23	
Y	12.0	18.1	11.4	18.1		17.1		17.7	22.2	23.4	24.0	48.8		20.0	20.7	15.4	

Table 1 (*continued*)

Number	02SX107*	02SX109	P09YMG1*	P09YMG2*	P09YMG3	07YX04	07YX05	07YX06	07FS01*	07FS02	03XWS01*	03XH05*	03XH06*	03XH04	03XH01	03XH03
Name	Yixingzhai dyke 1		Yanmenguan dyke			Shizhan dyke 1		Shizhan dyke 2	Yixingzhai dyke 2		Xiwangshan dyke 1	Xiwangshan dyke 2	Xiwangshan dyke 3	Xiwangshan dyke 4	Xiwangshan dyke 5	Xiwangshan dyke 6
SiO_2	50.48	50.74	51.65	51.65	49.18	50.83	51.01	49.69	50.67	50.76	48.22	48.84	47.95	51.12	49.88	51.88
TiO_2	1.57	0.94	1.58	1.59	0.76	0.97	0.88	0.74	1.40	1.22	2.20	2.35	2.30	1.29	1.38	1.25
Al_2O_3	13.19	14.40	14.66	14.63	14.21	13.05	13.22	13.64	13.55	13.62	12.66	12.97	12.73	13.33	14.06	13.26
FeO_t	15.0	12.2	14.7	14.7	12.6	14.6	14.0	14.1	14.3	13.7	20.1	20.1	19.9	15.5	15.0	14.8
MnO	0.22	0.19	0.18	0.18	0.21	0.22	0.21	0.22	0.19	0.20	0.27	0.28	0.27	0.22	0.22	0.22
MgO	5.78	7.00	4.16	4.13	7.13	6.81	6.97	7.57	7.01	7.11	4.51	4.37	4.35	6.39	5.74	6.48
CaO	9.71	10.70	7.21	7.44	10.49	10.02	9.96	10.33	9.47	9.53	9.10	9.20	9.16	10.28	10.61	10.24
Na_2O	1.98	2.50	2.99	2.95	3.33	2.02	2.06	2.30	2.13	2.28	2.24	2.24	2.28	2.27	2.28	2.39
K_2O	0.69	0.47	1.70	1.71	0.87	0.43	0.54	0.44	0.64	0.64	0.60	0.67	0.58	0.25	0.23	0.24
P_2O_5	0.25	0.14	0.47	0.47	0.11	0.11	0.10	0.09	0.23	0.20	0.37	0.37	0.43	0.13	0.16	0.13
LOI	0.65	0.15	0.16	0.08	0.46	0.68	0.90	0.68	0.34	0.60	0.67	1.18	0.98	0.37	1.03	0.82
Total	99.53	99.39	110.30	110.58	108.27	99.77	99.83	99.80	99.88	99.84	99.61	100.17	98.92	100.39	98.51	100.07
Rb	12.6	9.12	44.9	44.9	17.8	18.6	23.8		15.9		13.8	21.9	18.4	7.20	7.70	11.0
Sr	193	199	436	431	190	148	146		162		118	154	138	81.0	56.5	88.2
Ba	293	179	781	784	343	136	153		234		168	157	152	93.0	28.9	84.8
Th	1.34	1.62	3.99	3.73	0.42	0.69	0.55		1.70		1.37	1.23	1.91	0.39	1.41	0.55
U	0.36	0.16	0.52	0.50	0.08	0.14	0.16		0.36		0.58	0.58	0.76	0.39	0.47	0.38
Pb	4.96	2.23	9.55	9.22	9.15	2.86	2.79		5.05		1.85	2.51	3.40	1.21	1.58	1.83
Zr	97.5	47.1	166	164	51.1	71.2	67.1		126		217	257	255	86.7	87.9	78.1
Hf	3.23	1.51	4.80	4.65	1.52	2.06	1.92		3.43		5.90	7.07	7.65	2.43	2.59	2.42
Nb	4.47	2.13	8.53	8.51	2.55	3.64	3.42		5.96		1.79	5.34	12.2	2.96	4.61	3.99
Ta	0.51	0.36	0.46	0.46	0.17	0.22	0.22		0.36		0.26	0.23	0.90	0.40	0.35	0.31
Sc	43.5	35.7	29.9	21.9	45.1	50.0	48.6		43.6		–	40.1	29.3	–	41.1	43.4
V	346	217	260	255	243	290	272		316		–	392	409	–	312	301
Cr	84.4	95.7	64.1	62.4	171	66.1	68.3		149		26.3	26.5	36.2	52.5	47.4	72.5
Co	52.1	40.5	49.9	51.2	50.6	56.9	52.4		52.0		46.4	53.3	52.1	43.6	48.6	49.1
Ni	50.0	50.8	48.5	47.6	65.8	40.3	39.3		74.6		33.4	40.5	35.2	59.5	58.9	67.9
Cu	75.4	43.5	65.3	64.7	73.7	111	110		65.4		66.0	69.8	71.9	102	73.9	122
Be	0.60	0.22	1.19	1.21	0.33	0.49	0.49		0.75		—	10.9	0.94	–	0.53	0.58
Ga	19.0	15.2	23.1	22.7	15.5	15.8	16.0		18.4		19.9	21.5	20.3	16.6	16.8	17.3
Cs	0.45	0.38	0.75	0.73	0.22	2.48	2.90		0.72		0.14	0.29	0.53	0.08	0.38	0.43
Li	11.2	6.43	5.05	5.27	4.28	24.9	26.8		6.41		—	14.1	10.2	—	18.5	19.5
La	13.9	8.32	34.5	33.1	8.18	7.04	6.95		15.4		21.5	22.3	24.7	5.26	8.64	6.31
Ce	29.7	16.0	68.9	65.6	14.7	16.9	15.5		34.9		52.4	52.9	56.4	13.4	19.5	15.2
Pr	4.24	2.52	9.02	8.73	2.29	2.27	2.14		4.47		7.27	7.01	7.80	2.09	2.62	2.28
Nd	19.1	10.7	35.1	34.2	10.1	10.2	9.43		18.9		33.0	32.9	34.9	10.8	11.7	11.2
Sm	4.56	2.87	7.59	7.31	2.56	2.94	2.56		4.68		8.53	9.33	8.75	3.26	3.49	3.50
Eu	1.50	0.89	2.07	2.06	0.87	0.98	0.90		1.33		2.10	2.29	2.15	1.09	1.18	1.18
Gd	5.01	3.01	6.52	6.41	2.80	3.36	3.17		5.01		9.55	9.26	10.0	4.18	4.34	4.36
Tb	0.92	0.56	0.98	0.98	0.52	0.61	0.59		0.89		1.78	1.71	1.85	0.73	0.79	0.79
Dy	5.56	3.49	5.47	5.38	3.34	4.11	3.78		5.63		11.2	11.5	12.5	4.55	5.09	5.12
Ho	1.15	0.73	1.14	1.13	0.74	0.88	0.82		1.19		2.33	2.49	2.81	1.02	1.10	1.10
Er	3.27	2.10	3.03	3.01	2.04	2.49	2.31		3.24		7.11	6.88	7.84	2.83	3.10	3.02
Tm	0.53	0.35	0.45	0.43	0.30	0.39	0.35		0.48		1.00	1.09	1.15	0.44	0.46	0.45
Yb	3.33	2.22	2.84	2.75	1.99	2.53	2.28		3.05		6.58	7.13	7.52	2.84	2.99	2.83
Lu	0.52	0.36	0.43	0.42	0.31	0.39	0.35		0.46		1.07	1.19	1.18	0.46	0.46	0.41
Y	28.4	18.8	27.9	26.7	18.2	22.7	21.7		29.3		60.2	60.0	59.6	25.3	27.3	26.3

Notes: 1. FeO_t = total iron. 2. Entries with "–" represent data under determination. 3. Samples labeled with '*' are from coarse-grained parts (centers) of the intrusions, one sample with '**' (07DX10) is from a darksome enclave, one other with "***" (07DX11) is from a pegmatite vein inside the intrusion, and all the others are from fine-grained (chilled) margins.

Table 2
Nd and Sr isotopes of the Hengling, Yixingzhai and Xiwangshan dykes/sills in the North China Craton.
T_{DM} ages are calculated after DePaolo (1981).

Sample	Rb [ppm]	Sr [ppm]	$^{87}Rb/^{86}Sr$	$^{87}Sr/^{86}Sr$	2σ	$^{87}Sr/^{86}Sr_{(t1)}$	2σ	$^{87}Sr/^{86}Sr_{(t2)}$	2σ	Sm [ppm]	Nd [ppm]	$^{147}Sm/^{144}Nd$	$^{143}Nd/^{144}Nd$	2σ	$\varepsilon Nd_{(t1)}$	2σ	$\varepsilon Nd_{(t2)}$	2σ	fSm/Nd	T_{DM}	$\varepsilon Nd_{(0)}$
Hengling																					
SX009	14.27	484.94	0.0853	0.705260	0.000014	0.7026	0.0005	0.7028	0.0005	2.22	11.23	0.1198	0.511423	0.000009	−2.5	1.7	−4.0	1.6	−0.39	2.79	−23.7
03WT06	33.20	367.32	0.2600	0.710835	0.000014	0.7028	0.0007	0.7033	0.0007	3.84	18.19	0.1277	0.511502	0.000011	−3.2	1.8	−4.5	1.7	−0.35	2.90	−22.2
03WT10	23.54	375.90	0.1850	0.708723	0.000014	0.7030	0.0006	0.7034	0.0006	2.12	10.96	0.1169	0.511385	0.000010	−2.4	1.6	−4.0	1.5	−0.41	2.76	−24.4
07DX02	7.81	385.62	0.0586	0.704602	0.000011	0.7028	0.0005	0.7029	0.0005	2.81	10.04	0.1689	0.512397	0.000012	3.0	2.4	2.5	2.2	−0.14	2.55	−4.70
07DX04	6.20	237.94	0.0753	0.704842	0.000009	0.7025	0.0005	0.7027	0.0005	2.87	9.48	0.1830	0.512525	0.000012	1.6	2.6	1.3	2.4	−0.07	3.08	−2.20
07DX06*	6.09	763.30	0.0231	0.702105	0.000011	0.7014	0.0005	0.7014	0.0005	7.91	41.43	0.1155	0.511442	0.000012	−0.9	1.6	−2.5	1.5	−0.41	2.64	−23.3
07DX07*	29.79	709.32	0.1215	0.705149	0.000010	0.7014	0.0005	0.7016	0.0005	9.55	50.94	0.1133	0.511427	0.000011	−0.6	1.6	−2.2	1.5	−0.42	2.60	−23.6
07DX08	12.60	262.06	0.1391	0.707450	0.000011	0.7031	0.0005	0.7034	0.0005	2.89	10.49	0.1666	0.512291	0.000011	1.5	2.3	1.0	2.2	−0.15	2.76	−6.77
07DX09	15.76	316.14	0.1442	0.707387	0.000011	0.7029	0.0006	0.7032	0.0006	2.86	10.64	0.1624	0.512244	0.000011	1.8	2.3	1.1	2.1	−0.17	2.68	−7.68
07DX10**	0.00	74.59	0.0000	0.702695	0.000011	0.7027	0.0005	0.7027	0.0005	22.13	104.17	0.1284	0.511683	0.000012	0.2	1.8	−1.1	1.7	−0.35	2.61	−18.6
Yixingzhai																					
SX109	9.28	208.11	0.1281	0.706635	0.000014	0.7028	0.0005	0.7029	0.0005	2.43	9.63	0.1526	0.511951	0.000014	−1.7	2.1	−2.1	2.0	−0.22	2.97	−13.4
07YX04	21.33	143.16	0.4313	0.711637	0.000010	0.6988	0.0010	0.6992	0.0010	2.67	9.78	0.1651	0.512302	0.000011	1.8	2.2	1.6	2.2	−0.16	2.65	−6.55
07YX05	23.55	147.10	0.4634	0.714080	0.000010	0.7003	0.0010	0.7007	0.0010	2.64	9.62	0.1660	0.512282	0.000012	1.2	2.2	1.0	2.2	−0.16	2.76	−6.94
Xiwangshan																					
XWS01*	13.93	121.94	0.3286	0.713289	0.000014	0.7040	0.0008	0.7038	0.0008	8.36	31.09	0.1627	0.512162	0.000008	−0.7	2.1	−0.6	2.1	−0.17	2.93	−9.29
03XH01	3.33	48.42	0.1990	0.708389	0.000011	0.7027	0.0006	0.7027	0.0006	3.23	10.31	0.1894	0.512551	0.000008	0.2	2.4	0.2	2.5	−0.04	3.72	−1.69
03XH04	7.08	81.77	0.2508	0.710897	0.000010	0.7038	0.0007	0.7037	0.0007	5.86	22.32	0.1587	0.512194	0.000010	1.0	2.0	1.1	2.1	−0.19	2.63	−8.67
03XH06*	14.44	133.26	0.3136	0.712683	0.000009	0.7038	0.0008	0.7036	0.0008	2.10	6.34	0.1999	0.512606	0.000014	−1.4	2.6	−1.5	2.6	0.02	5.91	−0.62

Notes: 1. $\varepsilon Nd_{(0)}$, $\varepsilon Nd_{(t1)}$ ($^{87}Sr/^{86}Sr_{(t1)}$) and $\varepsilon Nd_{(t2)}$ ($^{87}Sr/^{86}Sr_{(t2)}$) are values at present day, time of crystallization (2147 Ma for Hengling, 2060 Ma for Yixingzhai, and 1973 Ma for Xiwangshan) and 2000 Ma ago, respectively. 2. Samples labeled with "*" are from coarse-grained parts of the intrusions, one sample with "**" (07DX10) is from a darksome enclave, and all the others are from fine-grained (chilled) margins.

2059.8 ± 4.7 Ma, respectively (Supplement data Table 2, Fig. 4). Extremely high Th and U contents (e.g., >2000 ppm) may bias U–Pb age results during SHRIMP performance, but it is thought to have no effect on the measurement of $^{207}Pb/^{206}Pb$ ages (Williams and Hergt, 2000). For other irregular grains, $^{207}Pb/^{206}Pb$ ages ranged from 1563 Ma to 1914 Ma with very large errors of 2–3% (Supplement data Table 2, Fig. 4). These irregular-shaped grains have an upper intercept age of ~1869 Ma (Fig. 4). It is likely that the 2060–2035 Ma ages represent times of igneous crystallization, because the corresponding grains show igneous textures (Fig. 4 inset), and because these ages are not shown by the wall rocks in direct contact with the dykes (e.g., GSBS, 2002). It is possible that the discordant age data of these two spots were generated by over-correction of common lead of a present-day composition, which was caused by small amounts of resin around the very small zircon grains during analyses; this would have little influence on $^{207}Pb/^{206}Pb$ ages. The 1563–1914 Ma ages reflect the time of metamorphic recrystallization, because the relevant grains show metamorphic textures, and because the ages are consistent with the major ~1850 Ma period of metamorphism known in this area (e.g., Guo et al., 2005; Zhao et al., 2001).

The Lu–Hf isotopes of the zircon grains of sample 02SX009 (one Hengling dyke) were analyzed, and the spots in Supplement data Table 3 are the same as the U–Pb analyses using SHRIMP II (Peng et al., 2005). The Lu–Hf data show $^{176}Lu/^{177}Hf$ of 0.00706 to 0.001609 and $^{176}Hf/^{177}Hf$ of 0.281330 to 0.281520, and yield $\varepsilon Hf_{(t)}$ values (t is given as the $^{207}Pb/^{206}Pb$ age of each spot obtained in Peng et al. (2005)), which vary from −5.5 to +2.2 (Supplement data Table 3). As the rock has undergone only low-grade metamorphism and the dates are interpreted as crystallization ages, the $\varepsilon Hf_{(t)}$ values probably represent the nature of the parent magma. Lu–Hf analysis could not be obtained for zircon grains from sample 02SX109 (from a Yixingzhai dyke) and zircon cores of sample 03XWS01 (an ~1973 Ma Xiwangshan dyke, Peng et al., 2005).

6. Whole-rock geochemistry

6.1. Significance of whole-rock compositions

Metamorphic and alteration processes have the potential to modify selectively whole-rock chemistry, manifested most obviously by a scatter of major elements and some large-ion lithophile elements (LILE) (e.g., Rb, Sr, Ba). In contrast, high field-strength elements (HFSE) and rare earth elements (REE) are relatively immobile during metamorphism, and in general tend to reflect igneous processes (Middelburg et al., 1988). However, during granulite facies metamorphism, Y, Zr, Th, U and REEs may also be modified (e.g., Bea and Montero, 1999; Villaseca et al., 2003). In this study, fresh samples were mostly selected from the margins of dykes/sills, and some from the centers; one sample was from a pegmatite vein in the Longwangtang sill (sample 07DX11), and another was from a pyroxenite enclave in the same pegmatite vein in this sill (sample 07DX10) (all indicated in Table 1). Most Hengling, Yixingzhai and Xiwangshan samples are tholeiitic in composition (Fig. 5a, b) and show narrow compositional variations (Fig. 6), whereas the REE and trace element patterns of samples from different parts of the intrusives in each swarm show diversity (Fig. 7).

Samples from the coarse-grained parts of the intrusives generally have lower concentrations of SiO_2, MgO and comparable elements (e.g., Ni, Cr), but higher TiO_2, P_2O_5 and most incompatible elements (e.g., La, Nb, Th, Zr) than the fine-grained chilled margins in the Hengling and Yixingzhai dykes/sills, and the fine-grained dykes of the Xiwangshan swarm (Figs. 5–7). We think that the fine-grained samples provide the compositions of the parental magmas of the intrusions, whereas the coarse-grained centers show more evolved compositions, or compositions that were altered during metamorphism/alteration, because the chilled margins were more resistant

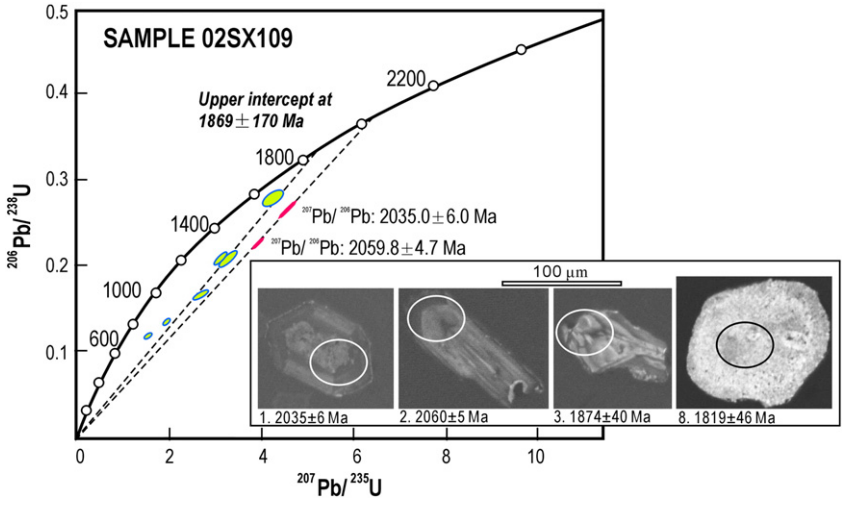

Fig. 4. U–Pb concordia diagram for sample 02SX109 from one of the Yixingzhai dykes. Inset: representative cathodoluminescence images of selected zircons.

to differentiation by quick solidification and to metamorphism or alteration due to their finer or cryptocrystalline textures. Thus, whole-rock compositions of the fine-grained samples (mostly from chilled margins) were used to estimate the primitive nature of the magmas that gave rise to the intrusions.

6.2. The Hengling sills/dykes

Samples from chilled margins of this sill/dyke swarm have high Mg tholeiitic basalt compositions (e.g., ~49 wt.% SiO_2 and 7–10 wt.% MgO) (Table 1; Fig. 6). Mg# (Mg numbers, calculated as Mg/(Mg + Fe) in molecular) values vary from 47 to 62. They have light REE enrichments ($La/Yb_N = 2.0–5.9$; Supplement data Table 4), compared with the heavy REEs (Fig. 7a, b), and they have negative anomalies in HFSEs (e.g., Th, U, Nb, Ta, Ti) on primitive mantle-normalized diagrams (Fig. 7a, b). They show no Eu-anomalies, but positive Sr-anomalies, mostly negative Zr-anomalies and negative Nb-anomalies (Fig. 7a, b).

The only sample (07DX10) from a pyroxenite enclave (Fig. 3j inset) of the Longwangtang sill has the typical composition of a cumulate (Supplement data Table 4; Fig. 6). The other two very coarse-grained samples (07DX06 and 07DX07) have distinctly higher concentrations/values of TiO_2 (~1.7 wt.%), P_2O_5 (~0.65 wt.%), La/Yb_N (13.5–13.9) and most trace elements, but they are lower in MgO (5.45–5.88 wt.%) and Zr/Zr* (0.11–0.13: $Zr/Zr^* = Zr_N/[(Nd_N)*(Sm_N)]^{1/2}$) than the chilled margins (Supplement data Table 4; Fig. 6). The pegmatite vein that entrained this pyroxenite enclave inside the Longwangtang sill has a diorite composition (e.g., ~57 wt.% SiO_2) (Table 1; Fig. 6).

The $^{87}Sr/^{86}Sr_{(t)}$ ratios of the Hengling rocks vary from 0.7014 to 0.7031 and $\varepsilon Nd_{(t)}$ values from −3.2 to +3.0 (t = 2147 Ma) (Table 2). The Nd T_{DM} ages (Nd-depleted mantle model ages, also referred to as 'crust-formation ages', were calculated with the depletion-mantle model, i.e., using the present-day value of a crustal sample and back through time when it had the isotopic composition of the depleted mantle reservoir) vary from 2.55 Ga to 3.08 Ga (Table 2).

6.3. The Yixingzhai dykes

Samples from chilled margins have tholeiitic basalt compositions (e.g., ~50 wt.% SiO_2 and ~7 wt.% MgO) (Table 1; Fig. 6). Mg# values range from 46 to 51. The margins have light REE enrichments ($La/Yb_N = 2.0–2.9$; Supplement data Table 4) and negative anomalies in HFSEs (e.g., Th, U, Nb, Ta, Ti) on primitive mantle-normalized diagrams (Fig. 7c, d). They have no Eu-anomalies, weakly negative to positive Sr-anomalies, and negative Zr- and Nb-anomalies (Fig. 7c, d). Samples from the middle of the intrusions have distinctly higher trace element concentrations and La/Yb_N ratios (3.0–8.7), but lower MgO (4.1–7.0 wt.%) and Sr/Sr* (0.51–0.72: $Sr/Sr^* = Sr_N/[(Pr_N)*(Nd_N)]^{1/2}$), compared with those from chilled margins (Supplement data Table 4; Fig. 6).

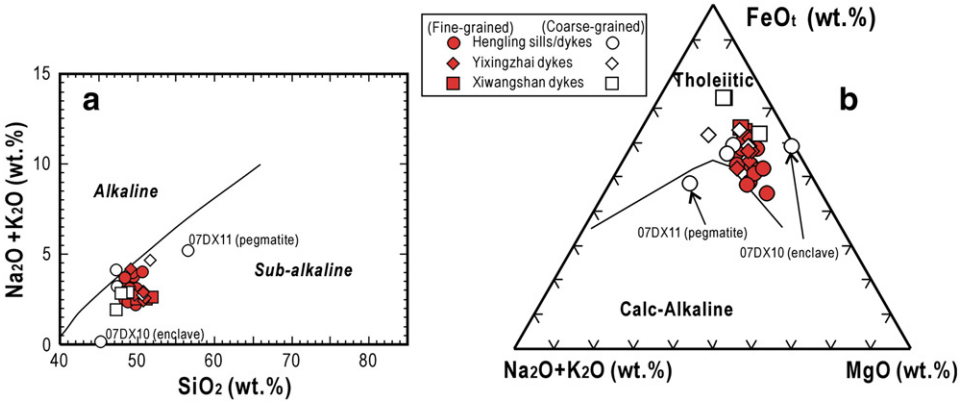

Fig. 5. (a) $Na_2O + K_2O$ vs. SiO_2 diagram, and (b) FeO_t–$Na_2O + K_2O$–MgO triangular diagram. After Irvine and Baragar (1971).

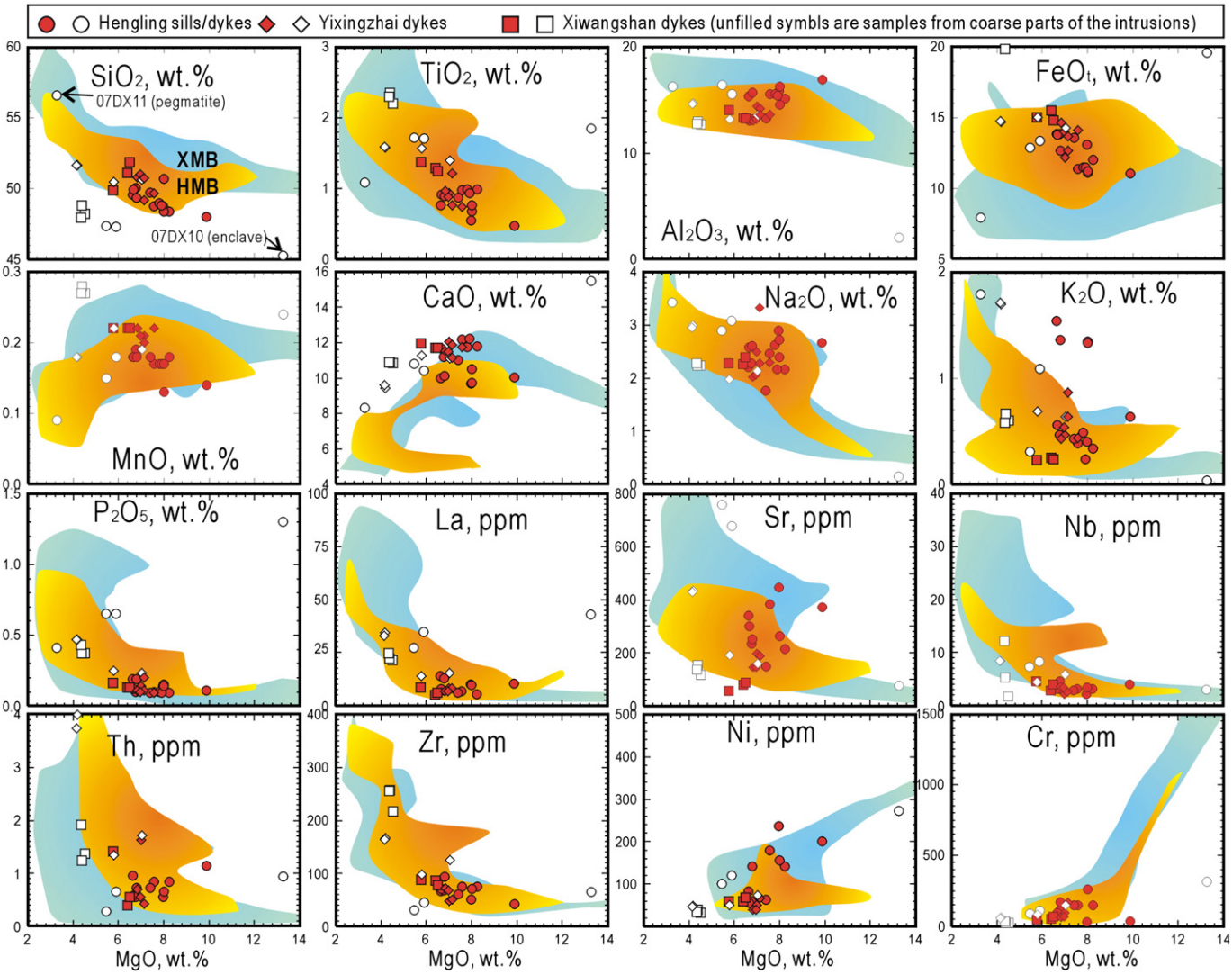

Fig. 6. Concentration variation diagrams of selected major oxides and trace elements versus MgO (wt.%) for the Hengling, Yixingzhai and Xiwangshan dykes/sills. The areas for igneous rocks in the Xuwujia magmatic belt (XMB) and the Hengling magmatic belt (HMB) are also shown.
Data of the XMB are from Peng et al. (2010, 2011, 2012a), whereas those of the HMB are from Du et al. (2011), Liu et al. (2012), Lu et al. (2006), and Sun and Hu (1993).

Samples of this dyke swarm have $^{87}Sr/^{86}Sr_{(t)}$ ratios from 0.6988 to 0.7028 and $\varepsilon Nd_{(t)}$ values from −1.7 to +1.8 (t = 2060 Ma) (Table 2). Their Nd T_{DM} ages vary from 2.65 Ga to 2.97 Ga (Table 2).

6.4. The Xiwangshan dykes

The Xiwangshan samples from fine-grained, thin (~1 m) dykes have tholeiitic basalt compositions (e.g., ~51 wt.% SiO_2 and ~6 wt.% MgO) (Table 1; Fig. 6). Mg# values vary from 41 to 45. The trace elements show light REE enrichments ($La/Yb_N = 1.3–2.1$) and negative anomalies in Nb, Ta and Sr, but the trace elements show enrichments in U compared with neighboring elements in a primitive mantle-normalized diagram (Fig. 7e, f). They have slightly negative Eu-anomalies, negative Sr- and Nb-anomalies, and slightly negative or no Zr-anomalies (Fig. 7e, f).

Samples from coarse-grained wider dykes (~2 m) have distinctly higher FeO_t, K_2O, trace element concentrations and La/Yb_N ratios (3.0–8.7), but lower SiO_2, MgO, CaO, Eu/Eu* (0.70–0.75: $Eu/Eu^* = Eu_N/[(Sm_N)*(Gd_N)]^{1/2}$) and Sr/Sr* (0.22–0.30) than those from the fine-grained thinner dykes (Supplement data Table 4; Fig. 6).

The $^{87}Sr/^{86}Sr_{(t)}$ ratios of the group vary from 0.7027 to 0.7040 and $\varepsilon Nd_{(t)}$ values range from −1.4 to +1.0 (t = 1973 Ma) (Table 2). The Nd T_{DM} ages are from 2.63 Ga to 3.72 Ga (with one abnormal value; Table 2).

7. Discussion

7.1. Petrogenesis of the Hengling, Yixingzhai and Xiwangshan dyke/sill swarms

7.1.1. The Hengling swarm

The centers of the Hengling intrusives have distinctly higher concentrations/values of TiO_2, P_2O_5, most trace elements and La/Yb_N, but lower MgO, Zr/Zr* and $\varepsilon Nd_{(t)}$, than the chilled margins (Tables 1 and 2; Figs. 6, 7a, b and 8a, b). These central compositions could represent late fractionates of plagioclase and clinopyroxene, or melts partly derived from the crust in view of their more enriched (lower) $\varepsilon Nd_{(t)}$ values. However, the samples from the margins with lower $\varepsilon Nd_{(t)}$ values do not show relatively lower MgO or higher SiO_2 contents (Fig. 8c, d), which would be expected if these lower values were induced by contamination of the ancient crust. The pyroxenite enclave (07DX10) from the Longwangtang sill is a cumulate of predominant clinopyroxene and minor magnetite (Fig. 3j). It has much lower Rb, Ba and Sr contents, but higher contents of most other trace elements than other samples from the main sill (Fig. 7a, b). Accumulation of

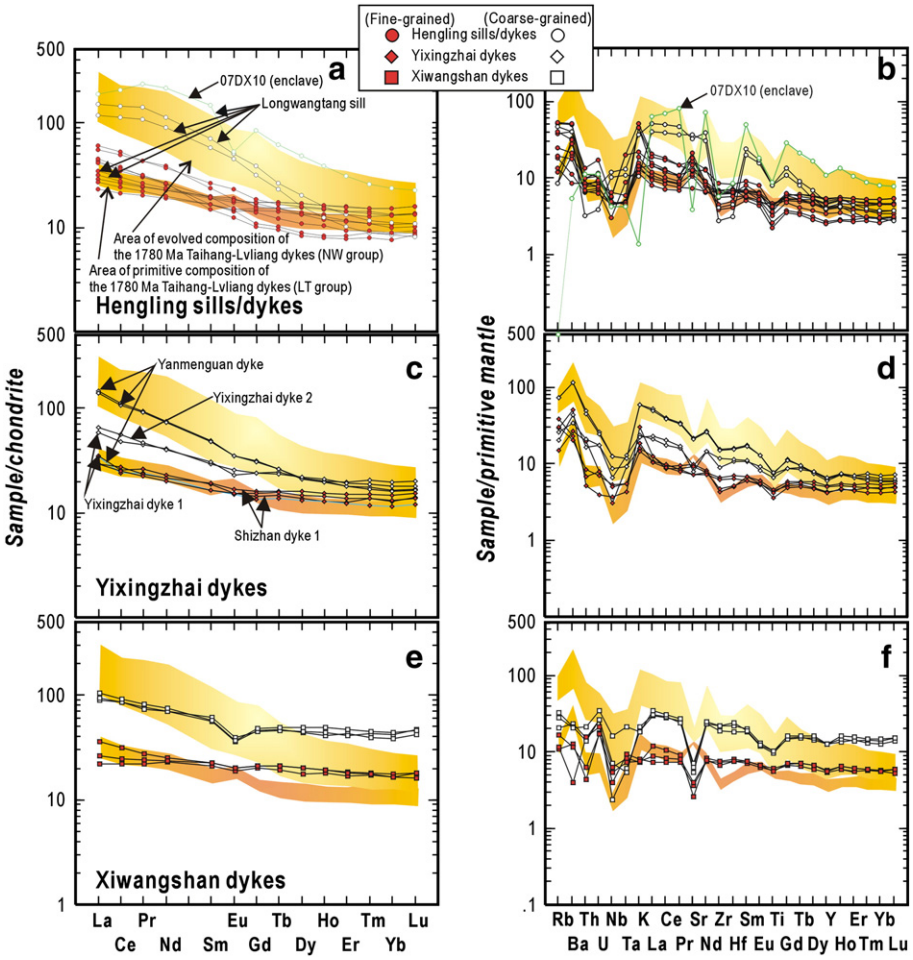

Fig. 7. Chondrite-normalized REE patterns (a) and primitive mantle-normalized trace element diagrams (b) for the Hengling, Yixingzhai and Xiwangshan dykes/sills. Areas for parental (LT Group) and evolved (NW Group) dykes of the craton-scale 1780 Ma Taihang–Lvliang dykes are also shown.
Data of the areas for parental (LT Group) and evolved (NW Group) dykes are of Peng et al. (2008). Chondrite and primitive mantle-normalized values are from Sun and McDonough (1989).

clinopyroxene from a basaltic magma would not have higher incompatible element concentrations and La/Yb_N values than its parent magma according to the coefficients of clinopyroxene (e.g., McKenzie and O'Nions, 1991) (Fig. 7a, b). We think that it is more likely that it fractionated from a more evolved magma (e.g., it was more like a cumulate from the late stage pegmatite vein that entrained this enclave), rather than it assimilated more crust than the rest of this sill.

The chilled margins have high Mg# (up to 62) and MgO (up to 9.9 wt.%), and thus are close to a primary composition (e.g., Frey et al., 1978). They have light REE enrichments ($La/Yb_N = 2.0–5.9$), negative anomalies in HFSEs (Fig. 7a, b), and mostly negative Zr- and Nb-anomalies. These compositions are similar to those of the parent magma (LT group) of the 1780 Ma mafic dyke swarm in the center of the NCC (Fig. 7a, b), which is most likely a melt that originated in the sub-continental lithospheric mantle (SCLM) of the NCC (Peng et al., 2008). These characteristics and the 2.55–3.08 Ga Nd T_{DM} ages suggest that the Hengling intrusions were also likely derived from the Archean SCLM of the NCC.

7.1.2. The Yixingzhai dyke swarm

The centers of the Yixingzhai dykes have distinctly higher trace element contents and La/Yb_N ratios but lower MgO and Sr/Sr* than the chilled margins (Supplement data Table 4; Fig. 6). This could be due to early fractionation of rock-forming minerals, e.g., plagioclase, which would have lower Sr/Sr* values. Due to limited chemical data, it is difficult to provide a precise evaluation of the contribution of crustal materials.

The parental magma of the Yixingzhai rocks, represented by samples of the chilled margins, is quite similar to that of the Hengling rocks (Figs. 5, 6, 7c, d, 8a, b), except that they have lower Mg# values (46–51), slightly lower Eu/Eu*(~0.93–0.99) and Sr/Sr* values (0.89–1.11), and variable $^{87}Sr/^{86}Sr_{(t)}$ ratios (0.6988 to 0.7028). We suggest that these rocks were also derived from the ancient SCLM of the NCC, similar to the Hengling rocks. Their lower Mg# and Eu/Eu* and Sr/Sr* values are either due to stronger differentiation and/or lower degrees of melting in the source region. And the abnormal $^{87}Sr/^{86}Sr_{(t)}$ values might be caused by alteration and metamorphism, e.g., due to Rb gain or Sr loss during fluid metasomatism.

7.1.3. The Xiwangshan dyke swarm

The coarse-grained Xiwangshan dykes have distinctly higher FeO_t, K_2O and trace element concentrations and La/Yb_N ratios, but lower SiO_2, MgO, CaO, Eu/Eu*, Sr/Sr* and $\varepsilon Nd_{(t)}$ ratios/concentrations than the fine-grained dykes (Supplement data Table 4; Figs. 6, 7e, f). These differences could be due to more differentiation, crustal contamination, and/or high-grade metamorphic alteration. Different degrees of crustal contamination are not likely the cause, because the coarser and more $\varepsilon Nd_{(t)}$-enriched dykes have lower SiO_2 concentrations than the fine-grained dykes (Fig. 8d), and they have similar trace element patterns (Fig. 7e, f). Both differentiation and late

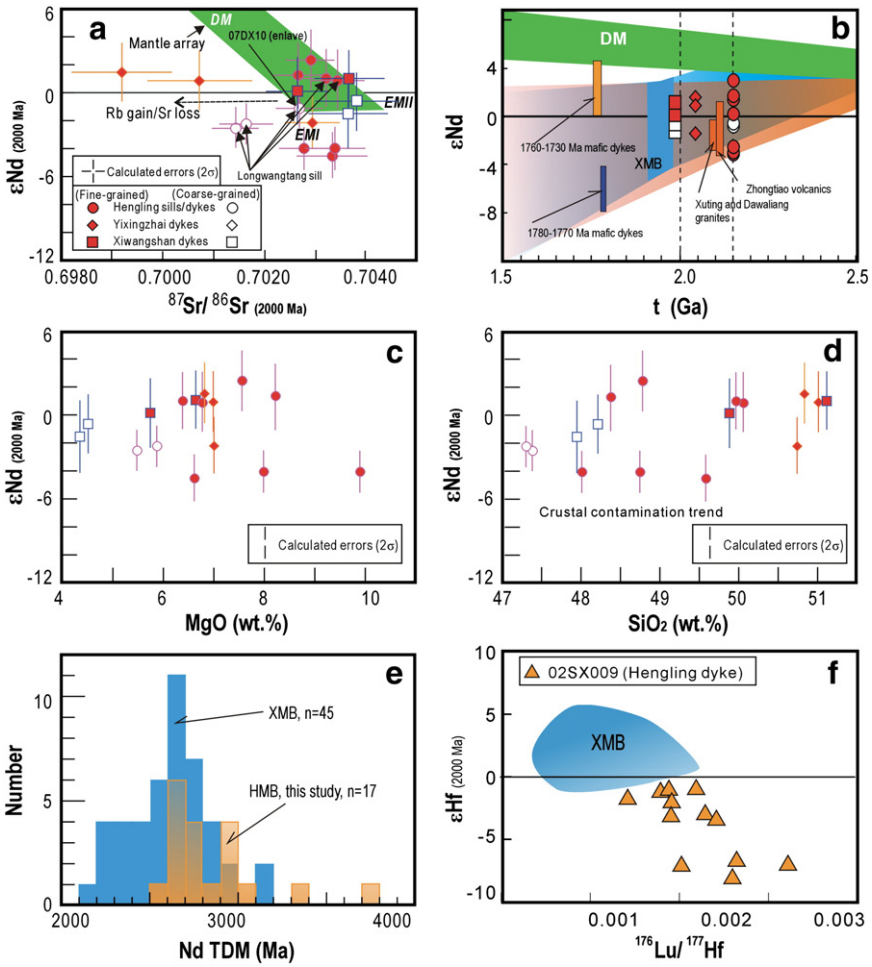

Fig. 8. (a) $\varepsilon Nd_{(2000\ Ma)}$ vs. $^{87}Sr/^{86}Sr_{(2000\ Ma)}$ diagram, (b) εNd vs. t (age, Ma) diagram, (c) $\varepsilon Nd_{(2000\ Ma)}$ vs. MgO (wt.%) diagram and (d) $\varepsilon Nd_{(2000\ Ma)}$ vs. SiO_2 (wt.%) diagram of the Hengling, Yixingzhai and Xiwangshan dykes/sills. (e) A histogram of the Nd model ages of igneous rocks from the Xuwujia magmatic belt; this study. (f) $\varepsilon Hf_{(t)}$ (t = 2000 Ma) vs. $^{176}Lu/^{177}Hf$ diagram. 'HMB' means Hengling magmatic belt.
Data of the Xuwujia magmatic belt (XMB) are from Peng et al. (2010, 2011, 2012a), whereas data of the Zhongtiao volcanics are from Sun and Hu (1993), data of the Xuting and Dawaliang granites are from Yang et al. (2011) and Zhao et al. (2011), and data of the 1780–1770 Ma and 1760–1730 Ma mafic dykes are from Peng et al. (2008, 2012b), respectively.

stage alteration could have contributed to these differences, considering the variations in major and trace elements, and the $\varepsilon Nd_{(t)}$ values.

Compared with the Hengling and Yixingzhai swarms, the Xiwangshan dykes have the lowest Mg# values (41–45) and light–heavy REE differentiation ($La/Yb_N = 1.3–2.1$), the highest heavy REE, Y and Zr concentrations, the most marked negative Sr-anomalies, and a unique U enrichment, although all three dyke swarms have similar isotopic characteristics (Figs. 6, 7e, f, 8a). Also, the trace element patterns of the Xiwangshan rocks are distinct from those of the craton-scale, 1780 Ma mafic dykes (Fig. 7e, f). However, their high Nd T_{DM} ages of > 2.5 Ga suggest that they were also possibly derived from the ancient SCLM of the NCC. The enrichments in U, heavy REE, Y and Zr might be a result of compositional metasomatism during granulite facies metamorphism as suggested by other comparable studies (e.g., Bea and Montero, 1999; Villaseca et al., 2003).

7.2. Genesis of the Hengling magmatic belt and a comparison with the Xuwujia belt

Fig. 9 is a simplified geological map of the eastern part of the NCC with the Phanerozoic strike-slip displacement of the Tan-Lu fault removed (using the offset estimated by Xu and Zhu, 1995), and the map also shows the distribution of all the 75 published ~2200–1880 Ma ages of intrusive and volcanic rocks from the NCC (see Supplement data Table 1 for references). These rocks are distributed in two belts: one with mostly 2200–2000 Ma volcanic and plutonic rocks termed here the Hengling magmatic belt (HMB); and another with mostly ~1960–1880 Ma igneous rocks — the Xuwujia magmatic belt (XMB) (Fig. 9). This subdivision is also supported by the aeromagnetic map of North China, which reveals near-surface lithologies and structures (Fig. 9 inset; Yuan, 2005).

According to their isotopic ages there are four generations of igneous rocks in the HMB (Fig. 10): the first ranges from ~2220 Ma to ~2120 Ma and contains possibly 4–5 cycles of mafic and felsic igneous rocks with a peak at ~2170 Ma, including the ~2147 Ma Hengling sills/dykes; the second ranges from ~2120 Ma to 2020 Ma and has probably about 4–5 cycles with a peak at 2090 Ma, including the ~2060–2035 Ma Yixingzhai dykes; the third is from 2020 Ma to 1960 Ma and contains a few igneous rocks including the ~1970 Ma Xiwangshan dykes; and the fourth is from ~1960 Ma to ~1880 Ma and comprises a few granitic rocks in the eastern margin of the NCC (North Korea) (Fig. 9). The mafic dykes/sills in the HMB, the Hengling, Yixingzhai and Xiwangshan swarms decrease in size from hundreds of meters to tens of meters to a couple of meters in width, and their frequencies and volumes progressively decrease, as shown in Fig. 10 and references listed in Supplement data Table 1. These three dyke/sill swarms have similar Sr–Nd isotopic characteristics, but they show a decrease in MgO contents and increasing concentrations of most trace elements through time (Tables 1–2; Figs. 6–8). These

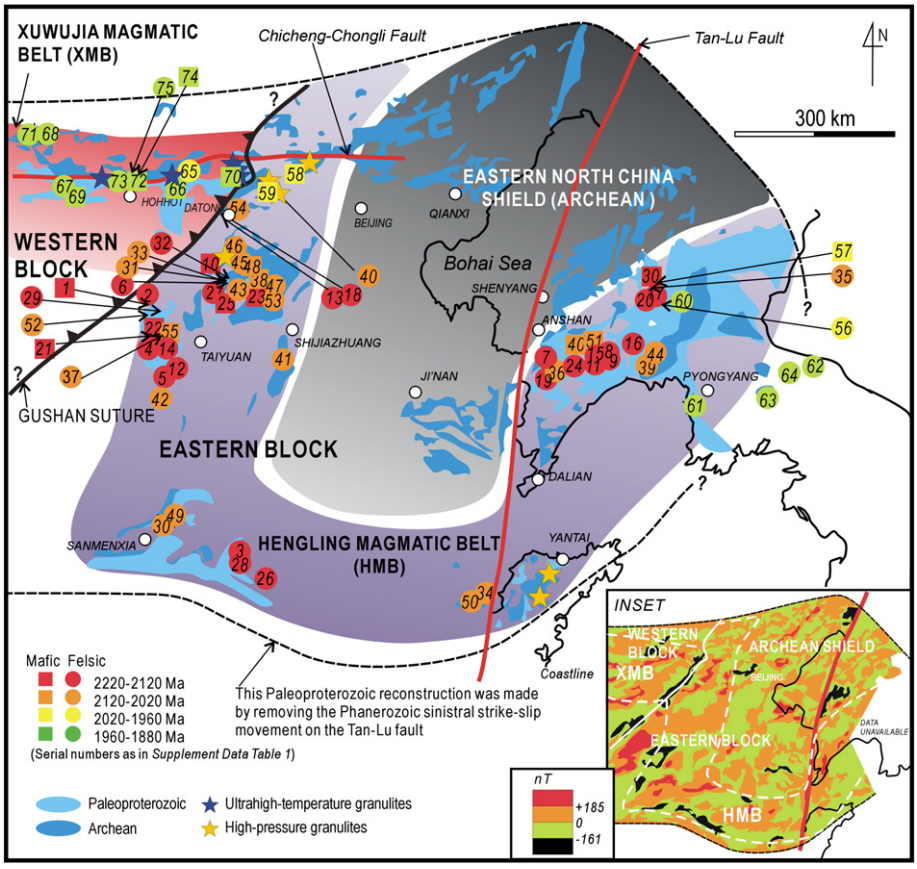

Fig. 9. Distribution of 2200–1880 Ma igneous rocks in the North China Craton: the rocks in the east and center constitute the Hengling magmatic belt, whereas the igneous bodies in the west of the craton comprise the Xuwujia magmatic belt. See Supplement data Table 1 for references. Inset: an aeromagnetic map of the North China Craton. Note: the outline of the North China Craton was reconstructed to Paleoproterozoic time after removal of Phanerozoic strike-slip movement on the Tan-Lu fault.
The inset is after Yuan (2005). Distance of the strike-slip offset is after Xu and Zhu (1995).

major variations probably originated from different degrees of melting in their different source regions. Fig. 12c shows that there could have been more and more melts from spinel lherzolite (in contrast to garnet lherzolite) in the source regions from the Hengling, to the Yixingzhai and Xiwangshan rocks. This could mean that the depths of the source regions in the HMB became shallower through time, if more garnet lherzolite is interpreted as a deeper source (e.g., Robinson and Wood, 1998). This modeling further suggests that the Hengling sills/dykes likely experienced up to 15% melting in their source region; the Yixingzhai rocks were about 10%, whereas the Xiwangshan rocks were much less than 10%, at ~5% (Fig. 12c). Furthermore, the decreasing Sr/Sr* and Nb/Nb* values, but increasing Th and

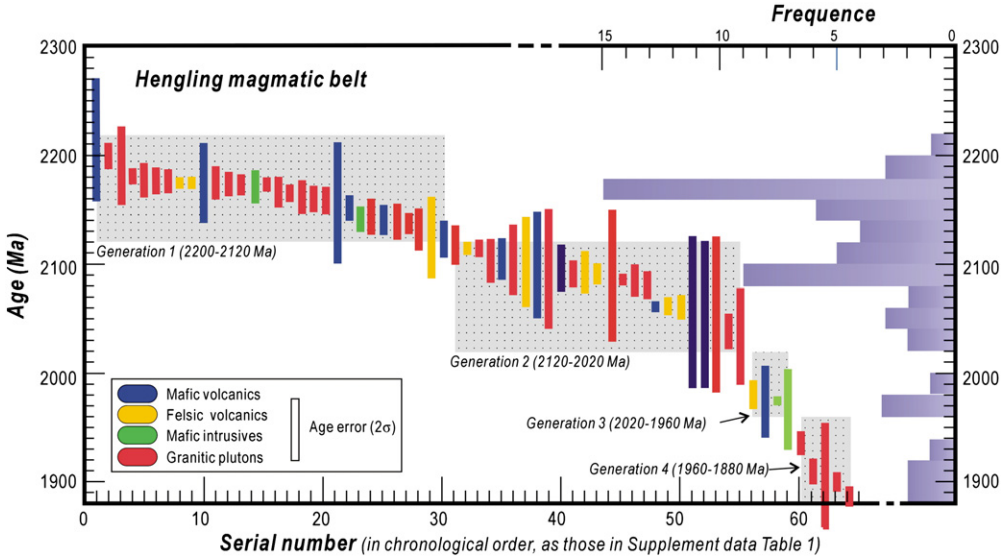

Fig. 10. Age distribution and histogram of the 2200–1880 Ga igneous rocks in the Hengling magmatic belt of the North China Craton. Serial numbers are as those in Supplement data Table 1 (see references therein).

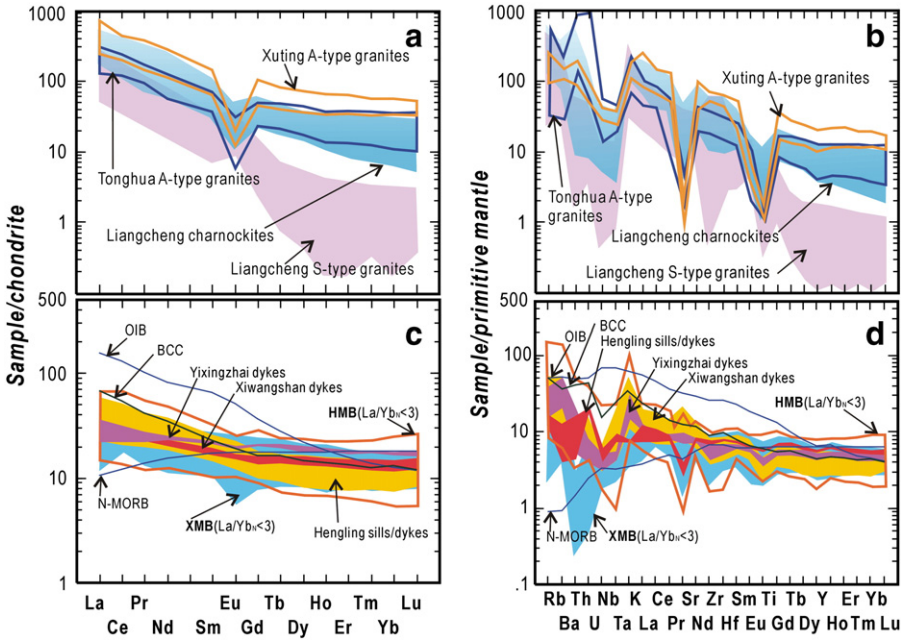

Fig. 11. Chondrite-normalized REE patterns (a, c) and primitive mantle-normalized trace element diagrams (b, d) of rocks in Hengling and Xuwujia magmatic belts. Data of Xuting granites and Tonghua granites are from Yang et al. (2011) and Lu et al. (2004b), respectively. Data of Liangcheng charnockites and S-type granites are from Peng et al. (2012a). Chondrite and primitive mantle-normalized values, and N-MORB (normal mid-ocean-ridge basalt), and OIB (ocean island basalt) are after Sun and McDonough (1989). Data of bulk continental crust are from Taylor and McLennan (1995). Selected ($La/Yb_N<3$) data of the XMB (Xuwujia magmatic belt) are from Peng et al. (2010, 2011, 2012a), whereas those of the HMB (Hengling magmatic belt) are after Du et al. (2011), Liu et al. (2012), and Lu et al. (2006).

U-concentrations, from Hengling to Xiwangshan may be due to more continental crust in their magmas, as well as to more extensive metasomatism involved in their higher grades of metamorphism (e.g., Bea and Montero, 1999; Villaseca et al., 2003) (Supplement data Table 4; Figs. 6–7). The granitic rocks in the HMB are mostly monzogranites and A-type granites, and the volcanic rocks vary in composition from mafic to felsic, or basic to intermediate to acidic. They generally have enriched compositions and could have originated from either ancient crust or the SCLM of the NCC (references of Supplement data Table 1).

The 1960–1880 Ma XMB in the western NCC comprises early gabbronorites and contemporaneous or slightly later charnockites, late S-type granites and basalts—basaltic andesites to rhyolite-dacites (Supplement data Table 1). In addition, ~1951 Ma carbonatite dykes occur in this area (Wan et al., 2008). These components were co-genetic and probably connected with the formation of the regional ultrahigh-temperature metamorphism (Peng et al., 2010, 2011, 2012a), which was likely at ~1930–1920 Ma (e.g., Liu et al., 2009a; Santosh et al., 2007a,b). The HMB and XMB rocks are distinctly separate in the Datong area as indicated by their ages (2200–1960 Ma vs. 1960–1880 Ma) and their geochemical signatures (Figs. 11–12). As regards the granitic rocks, the XMB is characterized by charnockites and S-type granites, whereas the HMB includes many monzogranites, A-type granites and tonalites (Supplement data Table 1; Fig. 11a, b). Considering the mafic components, the XMB is characterized by much lower Th, U, Nb, and Ta concentrations on a normalized trace element diagram (Fig. 11d), and has younger whole-rock Nd T_{DM} ages (Fig. 8e), and distinctly depleted Hf isotopes (of zircon grains) (Fig. 8f), than equivalent rocks in the XMB. Nb/Nb* vs. Zr/Zr* and Zr/Hf vs. Th/La diagrams (Fig. 12a, b) demonstrably separate the rocks in the two belts. A reasonable conclusion is that the igneous rocks in the XMB were derived from different magma sources, and they were generated from younger mantle regions than the HMB. These geochemical relations are also distinguishable by trace element patterns and isotopes from those of the ancient lithospheric mantle of the NCC, which is represented by the craton-scale 1780 Ma mafic dykes (Peng et al., 2008) and contemporaneous Xiong'er volcanics (Wang et al., 2010b). Moreover, based on a Sm/Yb vs. Sm diagram (Fig. 12c), the igneous rocks in the XMB probably had two kinds of origin: one from garnet lherzolite, and the other from both spinel lherzolite and garnet lherzolite, similar to the HMB. This possibly indicates that parts of the magmas of the XMB were derived from deeper and juvenile mantle sources than the HMB, except that some parts are similar (ancient and shallower, from the SCLM).

It is important to note that several granitic plutons, referred to as the fourth generation of the HMB in Fig. 10, occur in North Korea along the eastern margin of the NCC; they have similar ages as those in the XMB (Wu et al., 2007; Zhao et al., 2006). Although the published chemical compositions of these rocks are currently sparse, they are notably aluminous and are akin to similar S-type granites in the XMB. We suggest that these alumina-rich granites and the fourth generation of igneous rocks in the HMB had a similar mode of origin and were generated in a comparable tectonic environment as the equivalent rocks in the XMB. However, the position of the eastern boundary of the NCC in this particular area is still controversial.

7.3. Tectonic implications of the Hengling and Xuwujia magmatic belts

Comparing Fig. 9 with Fig. 1, it is clear that the boundary between the XMB and HMB is similar to the tectonic boundaries between the different blocks of the NCC in the areas studied by Kusky and Li (2003), Kusky et al. (2007), Peng et al. (2012a), Trap et al. (2007, 2011) and Zhao et al. (2005). And the XMB and HMB may be partly analogous to the Fengzhen mobile belt and the Jinyu + Liao-Ji belt, respectively of Zhai and Liu (2003) (Fig. 1). The fact that the Late Paleoproterozoic igneous suites (especially the mafic components) are mutually similar within the XMB and HMB, but distinctly different between each belt provides robust evidence that they belong to two different sub-blocks of the NCC, i.e., eastern and western blocks as shown in Fig. 9. However, the continuation of the borderline between the two magmatic belts under the major Cenozoic basins requires further study. The aeromagnetic map of China (inset in Fig. 9) suggests that this line is oriented SW–NE within the extremely low aeromagnetic anomalies, and is currently occupied by a deep fault (Yuan, 2005). In addition, the Archean basement in the northeast of the NCC contains few

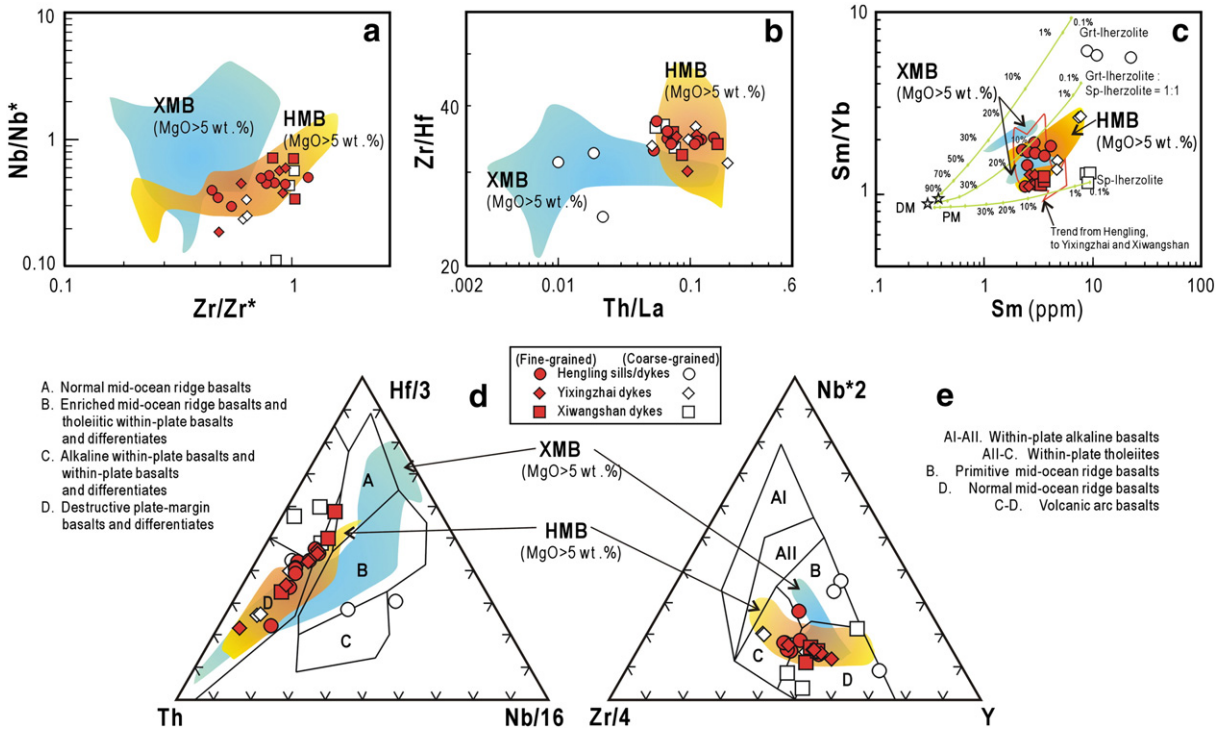

Fig. 12. (a) $Nb/Nb^* (=Nb_N/[(La_N)*(Th_N)]^{1/2})$ vs. $Zr/Zr^* (=Zr_N/[(Nd_N)*(Sm_N)]^{1/2})$ plot, (b) Zr/Hf vs. Th/La plot, (c) Sm/Yb vs. Sm diagram, (d) Hf/3–Th–Nb/16 diagram, and (e) Nb*2–Zr/4–Y diagram of the Hengling, Yixingzhai and Xiwangshan dykes/sills. Also plotted are selected (only those MgO > 5 wt.%) data of the Xuwujia magmatic belt (XMB) from Peng et al. (2010, 2011, 2012a) and the Hengling magmatic belt (HMB) from Lu et al. (2006), Du et al. (2011) and Liu et al. (2012). In c, the melt curves were calculated using the non-modal batch melting equations. Melt curves are drawn for spinel-lherzolite (with mode and melt mode of olivine(ol)$_{0.578}$ + orthopyroxene(opx)$_{0.270}$ + clinopyroxene(cpx)$_{0.119}$ + spinel(sp)$_{0.033}$ and ol$_{0.060}$ + opx$_{0.280}$ + cpx$_{0.670}$ + sp$_{0.110}$, respectively) and for garnet-lherzolite (with mode and melt mode of ol$_{0.598}$ + opx$_{0.211}$ + cpx$_{0.076}$ + garnet(grt)$_{0.115}$ and ol$_{0.030}$ + opx$_{0.160}$ + cpx$_{0.880}$ + grt$_{0.090}$). Mineral/matrix partition coefficients and DM (depleted mantle) and PM (primitive mantle) are from the compilation of McKenzie and O'Nions (1991). Three solid curves represent the melting trends starting from a DM source with lithologies of spinel-lherzolite, garnet-lherzolite, and a 1:1 mixing of spinel- and garnet-lherzolite. Degrees of partial melting based on a given source are marked beside the curves.

magmatic rocks; it could belong to the Archean basement (the Eastern North China Shield) of the eastern block (Fig. 9).

The mafic igneous rocks in the HMB are compositionally similar to those in modern volcanic arcs, whereas those in the XMB are similar to those from mid-oceanic ridges (Fig. 12d, e). Peng et al. (2010, 2011, 2012a) suggested that the igneous rocks in the XMB might be co-genetic with local ultrahigh-temperature metamorphism, and they resulted from ridge subduction processes between the eastern and western blocks of the NCC. In this model, minor amounts of ~2000 Ma granitic rocks and igneous-derived detrital zircon ages were interpreted to be of continental arc association. Peng et al. (2005) suggested that the Hengling dykes/sills were generated in a back-arc, the Xiwangshan dykes were post-collisional, and the Xuwujia dykes (in the XMB) intruded in an active continental margin.

We propose that the HMB dykes formed in an intra-continental environment instead of a volcanic arc, because: 1) their magma was derived from a mantle region as old as >2.5 Ga (Nd–Hf isotopes: Fig. 8e, f), which most likely was the SCLM of the NCC (c.f., Wu et al., 2005). Some may argue that the enriched Nd–Hf isotopes (Fig. 8e, f) originated from the assimilation of crustal material because the trace element patterns of the three dyke swarms show some similarity with that of the bulk continental crust (Fig. 11c, d). However, no significant contamination trend can be identified within each group of samples according to their parallel trace element patterns (Fig. 7) and variations in Nd isotopes (Fig. 8c, d). Also, their relatively high MgO but low SiO_2 contents (Fig. 6) suggests that there was no significant crustal assimilation either in the magma chamber or during intrusion. 2) The trace element patterns of the dyke magmas (Fig. 7) are similar to those of melts derived from the SCLM of the NCC, which was modified in the Late Archean (e.g., the ~1780–1760 Ma Xiong'er volcanic province: Wang et al., 2010b; and the Taihang giant mafic dyke swarms: Peng et al., 2008). Thus, their 'volcanic arc'-affinities originated in subcontinental lithospheric mantle. 3) Such tholeiitic mafic dyke swarms, as well as minor, contemporaneous, mafic to felsic volcanics and some A-type granites (Fig. 9) are generally produced in extensional environments (e.g., Hanski et al., 2006), and thus are notably different from calc-alkaline volcanic-dominated arc associations. The first two generations of the three dyke/sill swarms have contemporaneous volcanics and/or A-type granites in the HMB, e.g., the Hengling sills/dykes and volcanics in the Hutuo Supergroup (Du et al., 2010), A-type granites in the Liao-Ji area (Lu et al., 2004b), the Yixingzhai dykes and some volcanics in the Hutuo and Liaohe Groups (Jiang, 1987; Lu et al., 2006), the Dawaliang and Xuting A-type granites (Yang et al., 2011; Zhao et al., 2011), and the Xiwangshan dykes with volcanics in the Guanghua and Ji'an Groups (Lu et al., 2006).

Many authors have suggested that mafic volcanics and granites in the HMB were emplaced in an intra-continental rift, e.g., Sun and Hu (1993), Lu et al. (2006), Du et al. (2010, 2011), Yang et al. (2011), and Zhao et al. (2011). The decrease in the scale of magmatism of the mafic dykes/sills represented by the Hengling, Yixingzhai and Xiwangshan swarms, and the decreasing volumes of the magmatic products, based on the database in Supplement data Table 1 and Fig. 10, resulted from magmatism in this rift, which died out after 2000 Ma.

The geotectonic evolution of the NCC during the Paleoproterozoic was most likely as follows: 1) at ~2200 Ma an intra-continental rift was initiated in the Archean shield of the eastern block of the NCC (Fig. 13a), and the first three generations of magmatic rocks in the HMB were successively developed; 2) subduction began at 2100–2000 Ma and minor continental arc rocks evolved on the eastern margin of the western block and finally ridge subduction started at ~1960 Ma under the western block of the NCC, producing many intrusive ultramafic, mafic and felsic sills/dykes (the XMB), as well as ultrahigh-temperature metamorphism

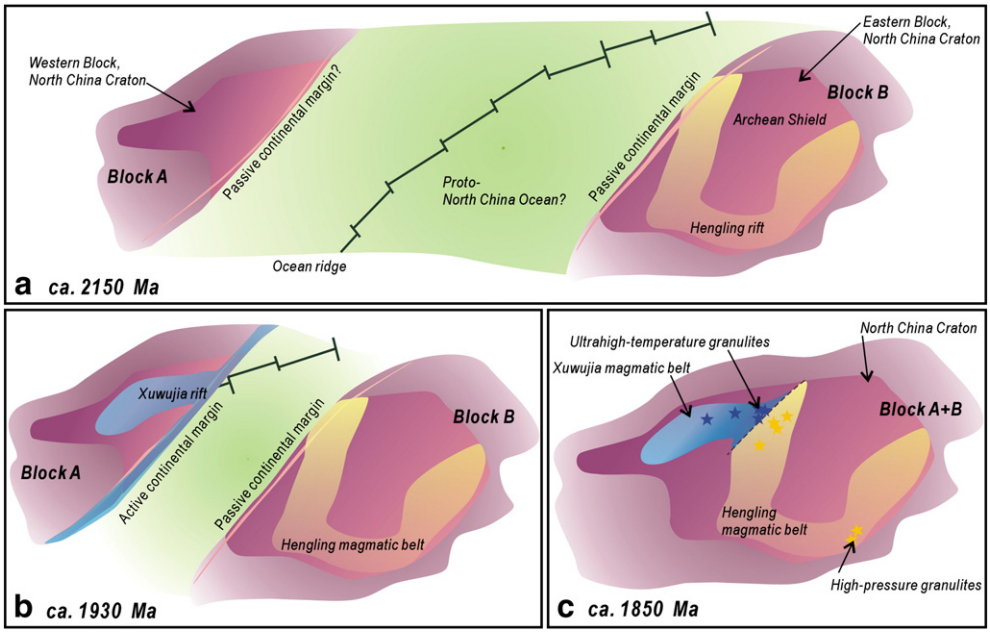

Fig. 13. Cartoons showing the proposed geological scenario and tectonic model of the North China Craton from ~2150 Ma (a), to ~1930 Ma (b), to ~1850 Ma (c). Blocks A and B are hypothetical continents, which included the western and eastern blocks of the North China Craton in the Paleoproterozoic, respectively.

in their host rocks (Guo et al., in press; Peng et al., 2012a). Conversely, magmatic evolution possibly ceased at ~1960 Ma in the HMB in the eastern block, leading to only minor granitic rocks in the far east of the HMB in North Korea during late closure of the rift (Fig. 13b); 3), the western and eastern blocks finally collided, giving rise to ~1850 Ma metamorphism up to high-pressure granulite facies in the suture zone, and in the rift (HMB) (e.g., Dong et al., 2010; Guo et al., 2005; Liu et al., 1998; Tam et al., 2010; Xie et al., 2011; Zhai et al., 1993; Zhao et al., 2001; Zhou et al., 2008). Uplift of this orogenic belt (most areas of the NCC) led to the final exhumation of the ~1930–1920 Ma ultrahigh-temperature metamorphic rocks and their high-grade wall rocks in the XMB, and to the ~1850 Ma high-pressure granulites to the east (Fig. 13c). This uplift also resulted in widespread ~1880–1790 Ma granitic rocks in the NCC (Geng et al., 2004; Lu et al., 2006; Wilde et al., 2002; Zhao et al., 2006, 2008a) and a subsequent craton-scale mafic dyke swarm at ~1780 Ma, followed by a long period of rifting at ~1780–1600 Ma (Peng et al., 2012b).

Collision of the blocks inside the NCC indicated by subduction-generated high-pressure granulite facies rocks has long been discussed (e.g., Trap et al., 2007, 2011, 2012; Zhai et al., 1993; Zhao et al., 2001, 2005), and different models have been proposed to interpret the ultrahigh-temperature metamorphism in the western block of the NCC, mainly based on the collision of two smaller blocks within the western block (e.g., Santosh et al., 2007a,b, 2012a,b; Zhai and Santosh, 2011; Zhao et al., 2005). In Fig. 13 we propose a new tectonic scenario starting at ~2200 Ma. The western block of the NCC underwent rifting and incipient ocean opening at ca. 1930 Ma. The rifted, but still coherent, western block of the Craton collided with the eastern block at ca. 1850 Ma, providing two different environments for the high-pressure and ultrahigh-temperature types of metamorphism. This model is consistent with published information and with our new data in this paper.

8. Conclusions

The 2200–1880 Ma igneous rocks (mafic and felsic, plutonic and extrusive) in the eastern block of the NCC constitute a new Hengling magmatic belt (HMB), which has distinct petrological assemblages and chemistry compared with the Xuwujia magmatic belt (XMB) in the western block of the Craton, which is mainly composed of 1960–1880 Ma gabbronorites, charnockites, S-type granites and volcanics. Three generations of tholeiitic mafic dykes/sills in the HMB, namely Hengling (~2147 Ma), Yixingzhai (~2060–2035 Ma) and Xiwangshan (~1973 Ma), experienced variable degrees of metamorphism from greenschist to high-pressure granulite facies, and are distinguished by their diagnostic occurrence and relic igneous textures. These rocks generally have enriched light REEs and negative anomalies in some HFSEs (e.g., Nb, Ta and Ti), compared with adjacent elements in primitive mantle-normalized diagrams. They have variable Eu- and Sr-anomalies, but mostly negative Zr- and Nb-anomalies. They have Nd T_{DM} ages of >2.5 Ga, indicating their origin in an ancient SCLM. The progressive changes in the chemical compositions of the three generations of dykes/sills further suggest that the depths of the source regions became progressively shallower with time, and the degrees of melting in the source regions tended to be successively lower through time. These rocks, as well as the A-type granites and other associations in this belt, most likely evolved in an intra-continental rift in the eastern block of the NCC. The changing size and scale of individual intrusions from Hengling to Yixingzhai and Xiwangshan, and the associated changes in magma volumes and diversity through time in the rift indicate that its climax was at ~2100 Ma and that it died out at ~2000 Ma. Previously, the XMB was thought to be the product of paleo-ridge subduction.

In our new model, the two magmatic belts (XMB and HMB) evolved within two different blocks of the NCC, i.e., the eastern and western blocks as previously proposed. In our model, production of the XMB by paleo-ridge subduction may have been responsible for the cessation of magmatism in the HMB, and the terminal collision and subsequent uplift likely resulted in the final exhumation of the igneous and metamorphic rocks, including the ultrahigh-temperature and high-pressure granulite facies rocks in different tectonic environments.

Supplementary data to this article can be found online at http://dx.doi.org/10.1016/j.lithos.2012.05.021.

Acknowledgments

This study was supported by the National Basic Research Program of China (973 Program; grant number 2012CB416601) and the National Natural Science Foundation of China (NSFC; grant numbers 41072146 and 41030316). Drs. Jian Zhang, Huafeng Zhang, Ruifu Zhao and Bo

Hu are thanked for their helpful discussions. We thank Drs. Andrew C Kerr, Shuwen Liu and one anonymous reviewer for their constructive comments.

References

Bea, F., Montero, P., 1999. Behavior of accessory phases and redistribution of Zr, REE, Y, Th, and U during metamorphism and partial melting of metapelites in the lower crust: an example from the Kinzigite Formation of Ivrea-Verbano, NW Italy. Geochimica et Cosmochimica Acta 63, 1133–1153.

Black, L.P., Kamo, S.L., Allen, C.M., Aleinikoff, J.N., Davis, D.W., Korsch, R.J., Foudoulis, C., 2003. TEMORA 1: a new zircon standard for Phanerozoic U–Pb geochronology. Chemical Geology 200, 155–170.

Chu, N.C., Taylor, R.N., Chavagnac, V., Nesbitt, R.W., Boella, R.M., Milton, J.A., German, C.R., Bayon, G., Burton, K., 2002. Hf isotope ratio analysis using multi-collector inductively coupled plasma mass spectrometry: an evaluation of isobaric interference corrections. Journal of Analytical Atomic Spectrometry 12, 1567–1574.

DePaolo, D.J., 1981. Nd isotopes in the Colorado Front Range and crust-mantle evolution in the Proterozoic. Nature 291, 193–196.

Dong, C.-Y., Wang, S.-J., Liu, D.-Y., Wang, J.-G., Xie, H.-Q., Wang, W., Song, Z.-Y., Wan, Y.-S., 2010. Late Paleoproterozoic crustal evolution of the North China Craton and formation time of the Jingshan Group: constraints from SHRIMP U–Pb zircon dating of meta-intermediate-basic intrusive rocks in eastern Shandong Province. Acta Petrologica Sinica 27, 1699–1706.

Du, L.-L., Yang, C.-H., Guo, J.-H., Wang, W., Ren, L.-D., Wan, Y.-S., Geng, Y.-S., 2010. The age of the base of the Paleoproterozoic Hutuo Group in the Wutai Mountains area, North China Craton: SHRIMP zircon U–Pb dating of basaltic andesite. Chinese Science Bulletin 55, 1782–1789.

Du, L.-L., Yang, C.H., Wang, W., Ren, L.-D., Wan, Y.-S., Song, H.-X., Geng, Y.-S., Hou, K.-J., 2011. The re-examination of the age and stratigraphic subdivision of the Hutuo Group in the Wutai Mountains area, North China Craton: evidences from geology and zircon U–Pb geochronology. Acta Petrologica Sinica 27, 1037–1055.

Frey, F.A., Green, D.H., Roy, S.D., 1978. Integrated models of basalt petrogenesis: a study of quartz tholeiites to olivine melilitites from South Eastern Australia utilizing geochemical and experimental petrological data. Journal of Petrology 19, 463–513.

Geng, Y.-S., Wan, Y.-S., Shen, Q.-H., Li, H.-M., Zhang, R.-X., 2000. Chronological framework of the Early Precambrian important events in the Lvliang area, Shanxi province. Acta Geologica Sinica 74, 216–223 (in Chinese with English Abstract).

Geng, Y.-S., Yang, C.-H., Song, B., Wan, Y.-S., 2004. Post-orogenic granites with an age of 1800 Ma in Lvliang Area, North China Craton: constraints from isotopic geochronology and geochemistry. Geological Journal of China Universities 10, 477–487 (in Chinese with English Abstract).

Geological Survey Bureau of Jilin (GSBJ), 2004. 1:250 000 geological map of the Tonghua area, Jilin.

Geological Survey Bureau of Shanxi (GSBS), 2002. 1:250 000 geological map of the Yingxian area, Shanxi.

Guo, S.-S., Li, S.-G., 2009. SHRIMP zircon U–Pb ages for the Paleoproterozoic metamorphic–magmatic events in the southeast margin of the North China Craton. Science in China, Series D: Earth Sciences 52, 1039–1045.

Guo, J.-H., Sun, M., Chen, F.-K., Zhai, M.-G., 2005. Sm–Nd and SHRIMP U–Pb zircon geochronology of high-pressure granulites in the Sanggan area, North China Craton: timing of Paleoproterozoic continental collision. Journal of Asian Earth Sciences 24, 629–642.

Guo, J.-H., Peng, P., Jiao, S.-J., Windley, B.F., in press. UHT sapphirine granulite metamorphism at 1.93–1.92 Ga caused by gabbronorite intrusions: implications for tectonic evolution of the northern margin of the North China Craton. Precambrian Research. http://dx.doi.org/10.1016/j.precamres.2011.07.020.

Hanski, E., Mertanen, S., Ramö, T., Vuollo, J. (Eds.), 2006. Dyke Swarms—Time Markers of Crustal Evolution. Taylor & Francis Publisher, London. 273 pp.

Iizuka, T., Hirata, T., 2005. Improvements of precision and accuracy in situ Hf isotope microanalysis of zircon using the laser ablation-MC-ICPMS technique. Chemical Geology 220, 121–137.

Irvine, T.N., Baragar, W.R.A., 1971. A guide to the chemical classification of the common volcanic rocks. Canadian Journal of Earth Sciences 8, 523–548.

Jiang, C.C., 1987. Precambrian Geology of Eastern Part of Liaoning and Jilin. Liaoning Science and Technology Publishing House, Shenyang.

Kröner, A., Wilde, S.A., Li, J.-H., Wang, K.-Y., 2005. Age and evolution of a late Archean to early Paleoproterozoic upper to lower crustal section in the Wutaishan/Hengshan/Fuping terrain of northern China. Journal of Asian Earth Sciences 24, 577–596.

Kröner, A., Wilde, S.A., Zhao, G.-C., O'Brien, P.J., Sun, M., Liu, D.-Y., Wan, Y.-S., Liu, S.-W., Guo, J.-H., 2006. Zircon geochronology and metamorphic evolution of mafic dykes in the Hengshan Complex of northern China: evidence for late Palaeoproterozoic extension and subsequent high-pressure metamorphism in the North China Craton. Precambrian Research 146, 45–67.

Kusky, T.M., Li, J.-H., 2003. Paleoproterozoic tectonic evolution of the North China Craton. Journal of Asian Earth Sciences 22, 383–397.

Kusky, T.M., Li, J.-H., Santosh, M., 2007. The Paleoproterozoic North Hebei Orogen: North China Craton's collisional suture with the Columbia supercontinent. Gondwana Research 12, 4–28.

Li, S.-Z., Zhao, G.-C., 2007. SHRIMP U–Pb zircon geochronology of the Liaoji granitoids: constraints on the evolution of the Paleoproterozoic Jiao–Liao-Ji belt in the Eastern Block of the North China Craton. Precambrian Research 158, 1–16.

Li, J.-H., Qian, X.-L., Huang, X.-N., Liu, S.-W., 2000. Tectonic framework of North China block and its cratonization in the Early Precambrian. Acta Petrologica Sinica 16, 1–10 (in Chinese with English abstract).

Li, S.-Z., Zhao, G.-C., Santosh, M., Liu, X., Dai, L.-M., Suo, Y.-H., Tam, P.-Y., Song, M.-C., Wang, P.-C., 2012. Paleoproterozoic structural evolution of the southern segment of the Jiao–Liao-Ji Belt, North China Craton. Precambrian Research 200–203, 59–73.

Liu, W.-J., Zhai, M.-G., Li, Y.-G., 1998. Metamorphism of the high-pressure basic granulites in Laixi, eastern Shandong, China. Acta Petrologica Sinica 14, 449–459 (in Chinese with English abstract).

Liu, S.-W., Pan, Y.-M., Xie, Q.-L., Zhang, J., Li, Q.-G., Yang, B., 2005. Geochemistry of the Paleoproterozoic Nanying granitic gneisses in the Fuping Complex: implications for the tectonic evolution of the Central Zone, North China Craton. Journal of Asian Earth Sciences 24, 643–658.

Liu, D.-Y., Wilde, S., Wan, Y.-S., Wu, J.-S., Zhou, H.-Y., Dong, C.-Y., Yin, X.-Y., 2008. New U–Pb and Hf isotopic data confirm Anshan as the oldest preserved segment of the North China Craton. American Journal of Science 308, 200–231.

Liu, S.-J., Santosh, M., Li, J.-H., 2009a. First application of the revised Ti-in-zircon geothermometer to Paleoproterozoic ultrahigh-temperature granulites of Tuguiwula, Inner Mongolia, North China Craton. Contributions to Mineralogy and Petrology 159, 225–235.

Liu, S.-W., Li, Q.-G., Liu, C.-H., Lü, Y.-J., Zhang, F., 2009b. Guandishan granitoids of the Paleoproterozoic Luliang metamorphic complex in the Trans-North China Orogen: SHRIMP zircon ages, petrogenesis and tectonic implications. Acta Geologica Sinica — English Edition 83 (3), 580–602.

Liu, C.-H., Zhao, G.-C., Sun, M., Zhang, J., He, Y.-H., Yin, C.-Q., Wu, F.-Y., Yang, J.-H., 2011. U–Pb and Hf isotopic study of detrital zircons from the Hutuo group in the Trans-North China orogen and tectonic implications. Gondwana Research 20, 106–121.

Liu, S.-W., Zhang, J., Li, Q.-G., Zhang, L.-F., Wang, W., Yang, P.-T., 2012. Geochemistry and U–Pb zircon ages of metamorphic volcanic rocks of the Paleoproterozoic Lvliang Complex and constraints on the evolution of the Trans-North China Orogen, North China Craton. Precambrian Research. http://dx.doi.org/10.1016/j.precamres.2011.07.006.

Lu, X.-P., Wu, F.-Y., Lin, J.-Q., Sun, D.-Y., Zhang, Y.-B., Guo, C.-L., 2004a. Geochronological successions of the Early Precambrian granitic magmatism in southern Liaoning Peninsula and its constraints on tectonic evolution of the North China Craton. Chinese Journal of Geology (Scientia Geologica Sinica) 39, 123–139 (in Chinese with English abstract).

Lu, X.-P., Wu, F.-Y., Zhang, Y.-B., Zhao, C.-B., Guo, C.-L., 2004b. Emplacement age and tectonic setting of the Paleoproterozoic Liaoji granites in Tonghua area, southern Jilin Province. Acta Petrologica Sinica 20, 381–392 (in Chinese with English abstract).

Lu, X.-P., Wu, F.-Y., Guo, J.-H., Wilde, S.A., Yang, J.-H., Liu, X.-M., Zhang, X.-O., 2006. Zircon U–Pb geochronological constraints on the Paleoproterozoic crustal evolution of the Eastern block in the North China Craton. Precambrian Research 146, 138–164.

McKenzie, D., O'Nions, R.K., 1991. Partial melt distributions from inversion of rare earth element concentrations. Journal of Petrology 32, 1021–1091.

Middelburg, J.J., van der Weijden, C.H., Woittiez, J.R.W., 1988. Chemical processes affecting the mobility of major, minor and trace elements during weathering of granitic rocks. Chemical Geology 68, 253–273.

O'Brien, P.J., Walte, N., Li, J.-H., 2005. The petrology of two distinct granulite types in the Hengshan Mts., China, and tectonic implications. Journal of Asian Earth Sciences 24 (5), 615–627.

Peng, Q.-M., Palmer, M.R., 2002. The Paleoproterozoic Mg and Mg–Fe borate deposits of Liaoning and Jilin Provinces, Northeast China. Economic Geology 97, 93–108.

Peng, P., Zhai, M.-G., Zhang, H.-F., Guo, J.-H., 2005. Geochronological constraints on the Paleoproterozoic evolution of the North China Craton: SHRIMP zircon ages of different types of mafic dikes. International Geology Review 47, 492–508.

Peng, P., Zhai, M.-G., Ernst, R., Guo, J.-H., Liu, F., Hu, B., 2008. A 1.78 Ga large igneous province in the North China Craton: the Xiong'er Volcanic Province and the North China dyke swarm. Lithos 101 (3–4), 260–280.

Peng, P., Guo, J.-H., Zhai, M.-G., Bleeker, W., 2010. Paleoproterozoic gabbronoritic and granitic magmatism in the northern margin of the North China Craton: evidence of crust–mantle interaction. Precambrian Research 183, 635–659.

Peng, P., Guo, J., Windley, B.F., Li, X., 2011. Halaqin volcano-sedimentary succession in the central-northern margin of the North China Craton: products of Late Paleoproterozoic ridge subduction. Precambrian Research 187, 165–180.

Peng, P., Guo, J., Windley, B.F., Liu, F., Chu, Z., Zhai, M., 2012a. Petrogenesis of Late Paleoproterozoic Liangcheng charnockites and S-type granites in the central-northern margin of the North China Craton: implications for ridge subduction. Precambrian Research. http://dx.doi.org/10.1016/j.precamres.2011.06.002.

Peng, P., Liu, F., Zhai, M., Guo, J., 2012b. Age of the Miyun dyke swarm: constraints on the maximum depositional age of the Changcheng System. Chinese Science Bulletin 57, 105–110.

Robinson, J.A.C., Wood, B.J., 1998. The depth of the spinel to garnet transition at the peridotite solidus. Earth and Planetary Science Letters 164, 277–284.

Santosh, M., 2010. Assembling North China Craton within the Columbia supercontinent: the role of double-sided subduction. Precambrian Research 178, 149–167.

Santosh, M., Tsunogae, T., Li, J.-H., Liu, S.-J., 2007a. Discovery of sapphirine-bearing Mg–Al granulites in the North China Craton: implications for Paleoproterozoic ultrahigh temperature metamorphism. Gondwana Research 11, 263–285.

Santosh, M., Wilde, S.A., Li, J.-H., 2007b. Timing of Paleoproterozoic ultrahigh-temperature metamorphism in the North China Craton: evidence from SHRIMP U–Pb zircon geochronology. Precambrian Research 159, 178–196.

Santosh, M., Liu, D.-Y., Shi, Y.-R., Liu, S.-J., 2012a. Paleoproterozoic accretionary orogenesis in the North China Craton: a SHRIMP zircon study. Precambrian Research. http://dx.doi.org/10.1016/j.precamres.2011.11.004.

Santosh, M., Liu, S.-J., Tsunogae, T., Li, J.-H., 2012b. Paleoproterozoic ultrahigh-temperature granulites in the North China Craton: implications for tectonic models on extreme crustal metamorphism. Precambrian Research. http://dx.doi.org/10.1016/j.precamres.2011.05.003.

Sun, D.-Z., Hu, W.-X. (Eds.), 1993. Precambrian Chronotectonic Framework and Chronological Crustal Structure of Zhongtiao Mt. Beijing. Geological Publication House, pp. 77–117 (in Chinese with English abstract).
Sun, S.-S., McDonough, W.F., 1989. Chemical and isotopic systematics of oceanic basalts implications for mantle composition and process. In: Saunders, A.D., Norry, M.J. (Eds.), Magmatism in the Ocean Basins: Geological Society of London, Special Publications, 42, pp. 313–354.
Tam, P.-Y., Zhao, G.-C., Liu, F.-L., Zhou, X.-W., Sun, M., Li, S.-Z., 2010. Timing of metamorphism in the Paleoproterozoic Jiao–Liao-Ji Belt: new SHRIMP U–Pb zircon dating of granulites, gneisses and marbles of the Jiaobei massif in the North China Craton. Gondwana Research 19, 150–162.
Taylor, S.R., McLennan, S.M., 1995. The geochemical evolution of the continental crust. Reviews of Geophysics 33, 241–265.
Trap, P., Faure, M., Lin, W., Monié, P., 2007. Late Paleoproterozoic (1900–1800 Ma) nappe stacking and polyphase deformation in the Hengshan–Wutaishan area: implications for the understanding of the Trans-North-China Belt, North China Craton. Precambrian Research 156, 85–106.
Trap, P., Faure, M., Lin, W., Augier, R., Fouassier, A., 2011. Syn-collisional channel flow and exhumation of Paleoproterozoic high pressure rocks in the Trans-North China Orogen: the critical role of partial-melting and orogenic bending. Gondwana Research 20, 498–515.
Trap, P., Faure, M., Lin, W., Le Breton, N., Monié, P., 2012. Paleoproterozoic tectonic evolution of the Trans-North China Orogen: toward a comprehensive model. Precambrian Research. http://dx.doi.org/10.1016/j.precamres.2011.09.008.
Villaseca, C., Martín Romera, C., De la Rosa, J., Barbero, L., 2003. Residence and redistribution of REE, Y, Zr, Th and U during granulite facies metamorphism: behaviour of accessory and major phases in peraluminous granulites of central Spain. Chemical Geology 200, 293–323.
Wan, Y.-S., Wilde, S., Liu, D.-Y., Yang, C.-X., Song, B., Yin, X.-Y., 2006. Further evidence for 1.85 Ga metamorphism in the Central Zone of the North China Craton: SHRIMP U–Pb dating of zircon from metamorphic rocks in the Lushan area, Henan Province. Gondwana Research 9, 189–197.
Wan, Y.-S., Liu, D.-Y., Xu, Z.-Y., Dong, C.-Y., Wang, Z.-J., Zhou, H.-Y., Yang, Z.-S., Liu, Z.-H., Wu, J.-S., 2008. Paleoproterozoic crustally derived carbonate-rich magmatic rocks from the Daqingshan area, North China Craton: geological, petrographical, geochronological and geochemical (Hf, Nd, O and C) evidence. American Journal of Science 308, 351–378.
Wan, Y.-S., Liu, D.-Y., Wang, S.-J., Dong, C.-Y., Yang, E.-X., Wang, W., Zhou, H.-Y., Du, L.-L., Yin, X.-Y., Xie, H.-Q., Ma, M.-Z., 2010. Juvenile magmatism and crustal recycling at the end of Neoarchean in western Shandong province, North China Craton: evidence from SHRIMP zircon dating. American Journal of Science 310, 1503–1552.
Wang, K.-Y., Wilde, S.-A., 2002. Precise SHRIMP U–Pb ages of Dawaliang granite in Wutaishan area, Shanxi Province. Acta Petrologica et Mineralogica 21, 407–411 (in Chinese with English abstract).
Wang, J., Wu, Y.-B., Gao, S., Peng, M., Liu, X.-C., Zhao, L.-S., Zhou, L., Hua, Z.-C., Gong, H.-J., Liu, Y.-S., 2010a. Zircon U–Pb and trace element data from rocks of the Huai'an Complex: New insights into the late Paleoproterozoic collision between the Eastern and Western Blocks of the North China Craton. Precambrian Research 178, 59–71.
Wang, X.-L., Jiang, S.-Y., Bai, B.-Z., 2010b. Melting of enriched Archean subcontinental lithospheric mantle: evidence from the ca. 1760 Ma volcanic rocks of the Xiong'er Group, southern margin of the North China Craton. Precambrian Research 182, 204–216.
Wang, Z.-H., Wilde, S., Wan, J.-L., 2010c. Tectonic setting and significance of 2.3–2.1 Ga magmatic events in the Trans-North China Orogen: new constraints from the Yanmenguan mafic–ultramafic intrusion in the Hengshan–Wutai–Fuping area. Precambrian Research 178, 27–42.
Wilde, S.A., 1998. SHRIMP U–Pb zircon dating of granites and gneisses in the Taihangshan–Wutaishan area: implications for the timing of crustal growth in the North China Craton. Chinese Science Bulletin 43, 144.
Wilde, S.A., Zhao, G.-C., Sun, M., 2002. Development of the North China Craton during the Late Archean and its final amalgamation at 1.8 Ga: some speculation on its position within a global Paleoproterozoic supercontinent. Gondwana Research 5, 85–94.
Wilde, S.A., Zhao, G.-C., Wang, K.-Y., Sun, M., 2003. SHRIMP zircon U–Pb age of the Hutuo Group in Wutai Mts.: new evidence for the Paleoproterozoic amalgamation of the North China Craton. Chinese Science Bulletin 48, 2180–2186 (in Chinese).
Wilde, S.A., Cawood, P.A., Wang, K.-Y., Nemchin, A.A., 2005. Granitoid evolution in the Late Archean Wutai Complex, North China Craton. Journal of Asian Earth Sciences 24, 597–613.
Williams, I.S., 1998. U–Th–Pb geochronology by ion microprobe. In: McKibben, M.A., Shanks III, W.C., Ridley, W.I. (Eds.), Applications of Microanalytical Techniques to Understanding Mineralizing Processes. Reviews in Economic Geology, 7. Society of Economic Geologists, pp. 1–35.
Williams, I.S., Hergt, J.M., 2000. U–Pb dating of Tasmanian dolerites: a cautionary tale of SHRIMP analysis of high-U zircon. In: Woodhead, J.D., Hergt, J.M., Noble, W.P. (Eds.), Beyond 2000: New Frontiers in Isotope Geoscience, Lorne; Abstracts and Proceedings, pp. 185–188.
Wu, F.-Y., Zhao, G.-C., Wilde, S.A., Sun, D.-Y., 2005. Nd isotopic constraints on crustal formation in the North China Craton. Journal of Asian Earth Sciences 24, 523–546.
Wu, F.-Y., Yang, Y.-H., Xie, L.-W., Yang, J.-H., Xu, P., 2006. Hf isotopic compositions of the standard zircons and baddeleyites used in U–Pb geochronology. Chemical Geology 234, 105–126.
Wu, F.-Y., Han, R.-H., Yang, J.-H., Wilde, S.A., Zhai, M.-G., Park, S.-C., 2007. Initial constraints on the timing of granitic magmatism in North Korea using U–Pb zircon geochronology. Chemical Geology 238, 232–248.
Wu, F.-Y., Zhang, Y.-B., Yang, J.-H., Xie, L.-W., Yang, Y.-H., 2008. Zircon U–Pb and Hf isotopic constraints on the Early Archean crustal evolution in Anshan of the North China Craton. Precambrian Research 167 (3–4), 339–362.
Xie, L.-W., Yang, J.-H., Wu, F.-Y., Yang, Y.-H., Wilde, S.A., 2011. PbSL dating of garnet and staurolite: constraints on the Paleoproterozoic crustal evolution of the Eastern Block, North China Craton. Journal of Asian Earth Sciences 42, 142–154.
Xu, J.-W., Zhu, G., 1995. Discussion on tectonic models for the Tan-Lu fault zone, Eastern China. Journal of Geology and Mineral Resources of North China 10, 121–133 (in Chinese).
Yang, D.-B., Xu, W.-L., Pei, F.-P., Wang, Q.-H., 2009. Petrogenesis of the Paleoproterozoic K-feldspar granites in Bengbu Uplift: constraints from petrogeochemistry, zircon U–Pb dating and Hf isotope. Earth Science — Journal of China University of Geosciences 34, 148–164 (in Chinese with English abstract).
Yang, C.-H., Du, L.-L., Ren, L.-D., Song, H.-X., Wan, Y.-S., Xie, H.-Q., Liu, Z.-X., 2011. The age and petrogenesis of the Xuting granite in the Zanhuang Complex, Hebei Province: constraints on the structural evolution of the Trans-North China Orogen, North China Craton. Acta Petrologica Sinica 27, 1003–1016 (in Chinese with English abstract).
Yu, J.-H., Wang, D.-Z., Wang, C.-Y., Li, H.-M., 1997. Ages of the Lvliang Group and its main metamorphism in the Lvliang Mountains, Shanxi: evidence from single-grain zircon U–Pb ages. Geological Review 43, 403–408 (in Chinese with English abstract).
Yuan, X.-C., 2005. Atlas of Geophysics in China. Geology Publishing House, Beijing. 216 pp.
Zhai, M.-G., Liu, W.-J., 2003. Paleoproterozoic tectonic history of the North China Craton: a review. Precambrian Research 122, 183–199.
Zhai, M.-G., Santosh, M., 2011. The early Precambrian odyssey of North China Craton: a synoptic overview. Gondwana Research 20, 6–25.
Zhai, M.-G., Guo, J.-H., Yan, Y.-H., Li, Y.-G., 1993. The discovery of high-pressure basic granulite in the Archean North China Craton and preliminary study. Science in China, Series B: Chemistry 36, 1402–1408.
Zhang, J., Zhao, G.C., Li, S.Z., Sun, M., Liu, S.W., Wilde, S.A., Kröner, A., Yin, C.Q., 2007. Deformation history of the Hengshan Complex: implications for the tectonic evolution of the Trans-North China Orogen. Journal of Structural Geology 29, 933–949.
Zhang, Y.-F., Liu, J.-T., Xiao, R.-G., Wang, S.-Z., Wang, J., Bao, D.-J., 2010. The hyalotourmalites of Houxianyu borate deposit in eastern Liaoning: zircon features and SHRIMP dating. Earth Science — Journal of China University of Geosciences 35, 985–999 (in Chinese with English abstract).
Zhang, J., Zhao, G.-C., Li, S.-Z., Sun, M., Chan, S.-L., Shen, W.-L., Liu, S.-W., 2012. Structural pattern of the Wutai Complex and its constraints on the tectonic framework of the Trans-North China Orogen. Precambrian Research. http://dx.doi.org/10.1016/j.precamres.2011.08.009.
Zhao, G.-C., Wilde, S.A., Cawood, P.A., Sun, M., 2001. Archean blocks and their boundaries in the North China Craton: lithological, geochemical, structural and P–T path constraints and tectonic evolution. Precambrian Research 107, 45–73.
Zhao, G.-C., Wilde, S.A., Cawood, P.A., Sun, M., 2002a. SHRIMP U–Pb zircon ages of the Fuping Complex: implications for Late Archean to Paleoproterozoic accretion and assembly of the North China Craton. American Journal of Science 302, 191–226.
Zhao, G.-C., Sun, M., Wilde, S.A., 2002b. Review of global 2.1–1.8 Ga orogens: implications for a pre-Rodinia supercontinent. Earth-Science Reviews 59, 125–162.
Zhao, G.-C., Sun, M., Wilde, S.A., Li, S.-Z., 2005. Late Archean to Paleoproterozoic evolution of the North China Craton: key issues revisited. Precambrian Research 136, 177–202.
Zhao, G.-C., Cao, L., Wilde, S.A., Sun, M., Choe, W.-J., Li, S.-Z., 2006. Implications based on the first SHRIMP U–Pb zircon dating on Precambrian granitoid rocks in North Korea. Earth and Planetary Science Letters 251, 365–379.
Zhao, G.-C., Wilde, S.A., Sun, M., Guo, J.-H., Kröner, A., Li, S.-Z., Li, X.-P., Zhang, J., 2008a. SHRIMP U–Pb zircon geochronology of the Huai'an Complex: constrains on Late Archean to Paleoproterozoic magmatic and metamorphic events in the Trans-North China Orogen. American Journal of Science 308, 270–303.
Zhao, G.-C., Wilde, S.A., Sun, M., Li, S.-Z., Li, X.-P., Zhang, J., 2008b. SHRIMP U–Pb zircon ages of granitoid rocks in the Lvliang Complex: implications for the accretion and evolution of the Trans-North China Orogen. Precambrian Research 160, 213–226.
Zhao, R.-F., Guo, J.-H., Peng, P., Liu, F., 2011. 2.1 Ga crustal remelting event in Hengshan Complex: evidence from zircon U–Pb dating and Hf–Nd isotopic study on potassic granites. Acta Petrologica Sinica 27, 1607–1623 (in Chinese with English abstract).
Zhou, X.-W., Zhao, G.-C., Wei, C.-J., Geng, Y.-S., Sun, M., 2008. EPMA U–Th–Pb monazite and SHRIMP U–Pb zircon geochronology of high-pressure politic granulites in the Jiaobei massif of the North China Craton. American Journal of Science 308, 328–350.